ORIGINAL RESEARCH ARTICLE

Syn-rift delta interfan successions: Archives of sedimentation and basin evolution

Bonita J. Barrett[1,2] | Rob L. Gawthorpe[2] | Richard E. Ll. Collier[1] | David M. Hodgson[1] | Timothy M. Cullen[1]

[1]School of Earth & Environment, University of Leeds, Leeds, UK

[2]Department of Earth Science, University of Bergen, Bergen, Norway

Correspondence
Bonita J. Barrett, School of Earth & Environment, University of Leeds, Leeds LS2 9JT, UK.
Email: eebbca@leeds.ac.uk

Abstract

Models that aim to capture the interactions between sediment supply, base level and tectonism recorded in fan delta successions in rift basins have not considered the stratigraphic archive preserved in interfan areas; yet interfan stratigraphy can provide a complementary record to the fan delta axes. The exhumed Early–Middle Pleistocene Kerinitis and Selinous fan deltas, in the hangingwall of the Pyrgaki–Mamoussia (P-M) Fault, Corinth Rift, Greece, offer an ideal laboratory for the assessment of interfan architecture. Furthermore, using the geometry of adjacent present-day fan deltas, interfans are classified into three end-members. The classification is based on their lateral separation, which determines the degree of interfingering of topset, foreset and bottomset deposits. Qualitative (facies, stratal geometries, nature of key surfaces) and quantitative (stratigraphic thickness, bedding dip, palaeocurrents, breakpoint trajectories) data were collected in the field and from unmanned aerial vehicle photogrammetry-based 3D outcrop models of the exhumed fan delta successions. The ancient Kerinitis–Selinous interfan architectures record: (a) initial westward progradation of the Kerinitis fan delta into the interfan area (Phase 1), (b) subsequent progradation of the Selinous fan delta into the interfan area and asymmetric growth of both fan deltas eastward (Phase 2), (c) stratal interfingering of foresets from both systems (Phase 3), and (d) relative base-level fall, erosion and reworking of sediments into the interfan area (Phases 4 and 5). The Kerinitis–Selinous interfan evolution is linked to initial net subsidence of the P-M Fault (Phases 1–3) and subsequent net uplift (Phases 4 and 5) resulting from a northward shift in fault activity. The interfan area provides a more complete stratigraphic record than the proximal axial areas of the fan deltas of the early stages of basin uplift, through higher preservation potential and protracted submergence. Therefore, for the most comprehensive insight into basin evolution, interfan analysis should be undertaken in concert with analysis of the fan delta axes.

KEYWORDS
Basin evolution, fan delta, interfan, stratigraphy, syn-rift.

1 | INTRODUCTION

The sedimentary successions preserved between adjacent, contemporaneous fluvial, deltaic or deep water fan systems (Figure 1) preserve an alternative stratigraphic archive to the fan axes (Higgs, 1990; Hook *et al.*, 2003; Bhiry and Occhietti, 2004; Leppard and Gawthorpe, 2006; Assine *et al.*, 2015; Turner and Connell, 2018). The interfan area is defined here as the area between two lines that project from the apices of two fan deltas to their intersection at the most distal point of bottomset interfingering (Figure 1). In this area, the fans coalesce from the proximal to distal parts. Identification of the most distal point of bottomset interfingering in modern and ancient systems is challenging, and as such the definition can be considered a theoretical, rather than a measurable limit.

The interfan areas between fan deltas may record the sedimentary response to relative base-level changes, yet are unstudied and therefore remain a missing piece in the published conceptual models that aim to capture the interactions of sediment supply, base level and tectonism in rift basins (Leeder and Gawthorpe, 1987; Gawthorpe *et al.*, 1994, 1997; Gawthorpe and Leeder, 2000; Leeder *et al.*, 2002; Young *et al.*, 2002). The interfan offers a complementary stratigraphic record to the fan delta axes of relative base-level change and tectono-sedimentary evolution. For example, during a relative base-level fall, the fan delta axis may become exposed and degraded, but the deeper and more sediment-starved interfan will remain submerged and thus preserve a more complete record of sedimentation and

basin evolution. The frontal deepwater setting along the fan delta axis may also record this transition in deepwater sediments, but the interfan area captures the interaction of two adjacent fan deltas through basinal change, as well as offering a more proximal record. The key regressive and transgressive surfaces that mark the pivotal moments in relative base-level change can also be expressed differently (e.g. suppressed erosion or thicker condensed intervals) and may be diachronous (Barrett *et al.*, 2018). Thus, a better grasp of interfan sedimentary facies, architecture and stratal surfaces would allow a more complete understanding of along-strike interactions between adjacent fan deltas during basin evolution.

The southern shore of the Gulf of Corinth (Figure 2) offers an ideal field laboratory for exploring interfan architectures, as there are a series of modern fan deltas along the coast, Late Pleistocene lowstand fan deltas that are submerged and imaged in bathymetry data, and a number of exhumed syn-rift fan deltas that formed along normal faults since ~1.8 Ma (Ford *et al.*, 2016; Gawthorpe *et al.*, 2017a). A number of studies focus upon the stratigraphic architecture of the Early–Middle Pleistocene Gilbert-type fan deltas in the Gulf of Corinth: Evrostini/Ilias (Zelilidis and Kontopoulos, 1996; Zelilidis, 2003; Rohais *et al.*, 2007a, 2008; Gobo *et al.*, 2014, 2015), Kryoneri (Gawthorpe *et al.*, 2017b), Vouraikos (Ford *et al.*, 2007), Kerinitis (Ori *et al.*, 1991; Poulimenos *et al.*, 1993; Dart *et al.*, 1994; Gawthorpe *et al.*, 1994; Backert *et al.*, 2010; Gawthorpe *et al.*, 2017b) and Selinous fan deltas (Poulimenos *et al.*, 1993; Barrett *et al.*, 2019). These studies highlight the
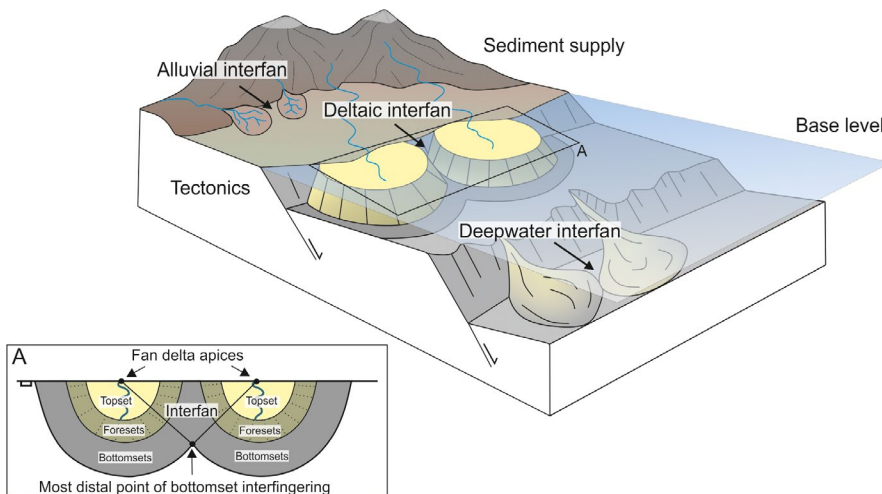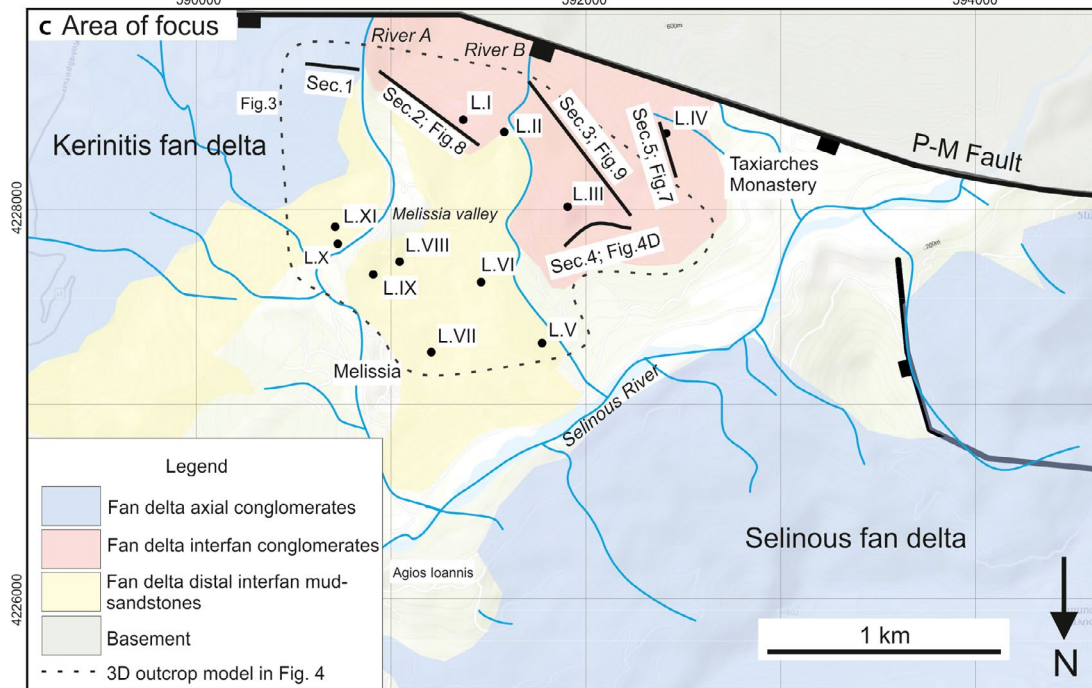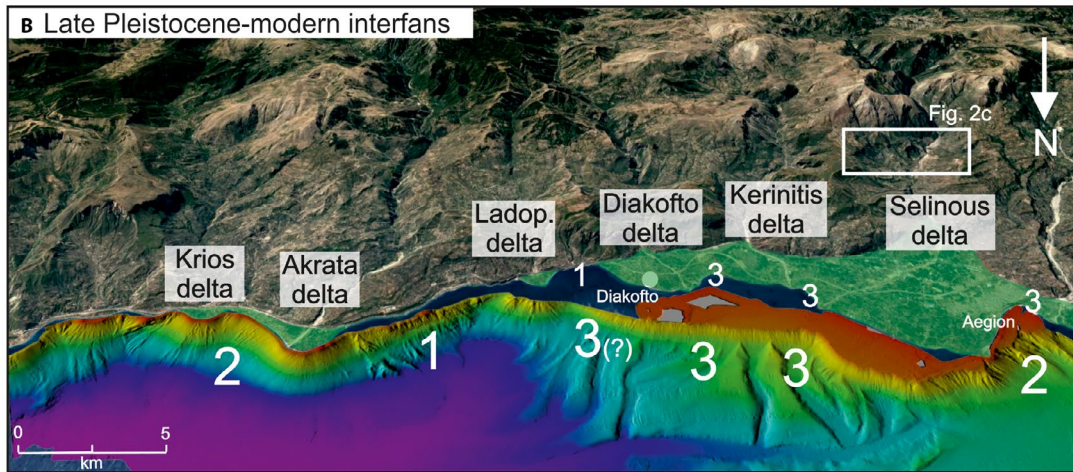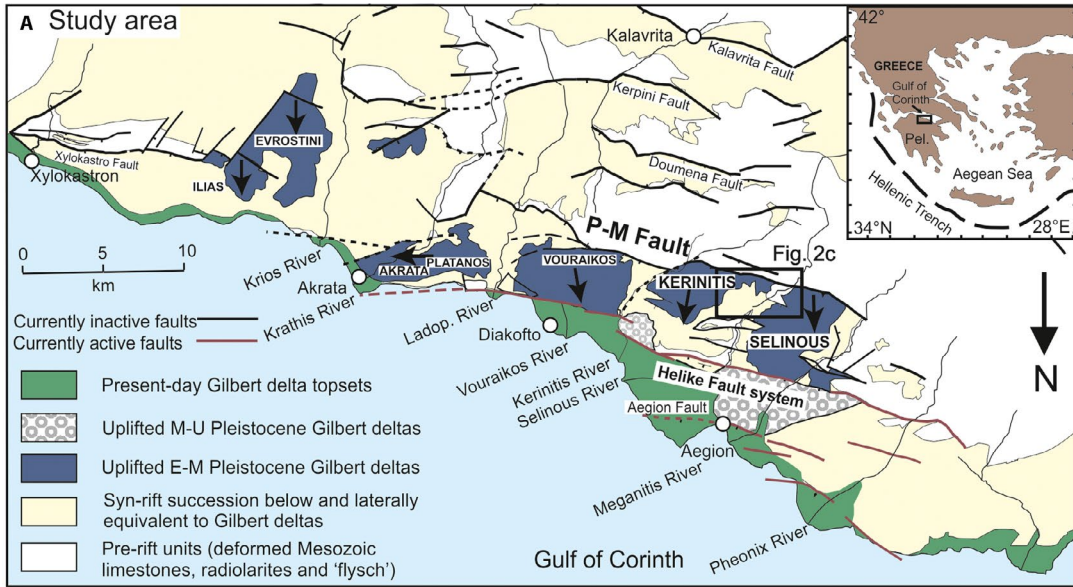

FIGURE 1 Source-to-sink block model with interfan areas highlighted in alluvial, deltaic and deepwater settings. (A) Deltaic interfans more specifically defined as the area between two lines that project from the two fan delta apices to their intersection at the most distal point of bottomset interfingering.

FIGURE 2 (A) Location map of southern shore of the Gulf of Corinth with the Early–Middle Pleistocene Kerinitis and Selinous fan deltas highlighted. Modified from Barrett et al. (2018) after Ford et al. (2010, 2007, 2013), Ghisetti and Vezzani (2004) and Gawthorpe et al. (2017a). (B) Modern fan deltas on topographic map (Google Earth) and Late Pleistocene examples imaged in bathymetry data. Numbers denote interfan classification according to scheme in Figure 11. Bathymetry data from McNeill et al. (2005) and Cotterill (2002). (C) Area of focus with key sections and localities indicated. Position of (C) is indicated in (A) and (B). Pel. = Peloponnesus.

A Study area

Kalavrita
Kalavrita Fault
Kerpini Fault
Doumena Fault
P-M Fault
Fig. 2c
GREECE
Gulf of Corinth
Pel.
Aegean Sea
Hellenic Trench
42°
34°N
28°E
Xylokastro Fault
Xylokastron
EVROSTINI
ILIAS
Krios River
AKRATA
PLATANOS
Akrata
Krathis River
VOURAIKOS
KERINITIS
SELINOUS
Helike Fault system
Aegion Fault
Ladop. River
Diakofto
Vouraikos River
Kerinitis River
Selinous River
Aegion
Meganitis River
Pheonix River
Gulf of Corinth
N

0 5 10
km

Currently inactive faults
Currently active faults

Present-day Gilbert delta topsets
Uplifted M-U Pleistocene Gilbert deltas
Uplifted E-M Pleistocene Gilbert deltas
Syn-rift succession below and laterally equivalent to Gilbert deltas
Pre-rift units (deformed Mesozoic limestones, radiolarites and 'flysch')

B Late Pleistocene-modern interfans

N
Fig. 2c
Ladop. delta
Diakofto delta
Kerinitis delta
Selinous delta
Krios delta
Akrata delta
Diakofto
1
3
3
3
Aegion
2
1
3 (?)
3
3
2

0 5
km

590000 592000 594000

C Area of focus

River A
River B
Sec. 1
Fig. 3
Sec. 2; Fig. 8
L.I
L.II
Sec. 3; Fig. 9
Sec. 5; Fig. 7
L.IV
P-M Fault
Kerinitis fan delta
L.III
Taxiarches Monastery
L.XI
Melissia valley
L.X
L.VIII
L.VI
Sec. 4; Fig. 4D
L.IX
L.VII
L.V
Melissia
Selinous River
Agios Ioannis
Selinous fan delta

4228000
4226000

Legend
Fan delta axial conglomerates
Fan delta interfan conglomerates
Fan delta distal interfan mud-sandstones
Basement
3D outcrop model in Fig. 4

1 km
N

sedimentary facies distribution and sequence stratigraphic relationships within these deposits, and the role of tectonics, lake level and sediment supply on fan delta development. However, none of these studies address the interfan areas between the fan deltas.

Here, the focus is placed upon the interfan area between the Early–Middle Pleistocene, Selinous and Kerinitis syn-rift fan deltas located in the immediate hangingwall of the Pyrgaki–Mamoussia (P-M) Fault. Geometric observations from the associated modern and Late Pleistocene submerged fan deltas are used to inform the analysis. The aim of this paper is to advance our understanding of along-strike interactions in syn-rift settings through analysis of interfan stratigraphy. Using field data and UAV photogrammetry-based 3D outcrop models, the objectives of the study are to: (a) describe and interpret the Kerinitis–Selinous (K–S) interfan evolution from the stratigraphic architecture and sedimentology; (b) propose a classification scheme for ancient interfans based on modern delta geometries; (c) discuss the mechanisms for the observed asymmetry in the ancient and modern fan deltas, and the value of including interfan analysis in sedimentary basin analysis.

2 | STUDY AREA

The Corinth Rift was activated at ~5 Ma (Collier and Dart, 1991; Leeder et al., 2008) and currently accommodates extension rates of up to 5–10 mm/year across the Gulf of Corinth (Clarke et al., 1997; Briole et al., 2000; Avallone et al., 2004; Floyd et al., 2010). The locus of faulting on the southern coast of the present gulf has migrated northwards over time (Goldsworthy and Jackson, 2001; Leeder et al., 2008; Ford et al., 2013, 2016; Nixon et al., 2016), recording two major rifting phases (Rohais and Moretti, 2017; Gawthorpe et al., 2017a). Rift 1 occurred from 5–3.6 Ma to 2.2–1.8 Ma, and strain was accommodated on the present-day onshore faults. In the west, activity was focussed upon the Kalavrita Fault in Northern Peloponnesos, before activity migrated basinwards onto the P–M Fault (study area, Figure 2) at ~1.8 Ma (Ford et al., 2016; Gawthorpe et al., 2017a). Rift Phase 2 commenced, and the Kerinitis and Selinous fan deltas formed, before activity migrated from the P–M Fault onto the Helike Fault system around ~0.8 Ma (Ford et al., 2013). Today, strain is primarily accommodated on faults offshore in the Gulf of Corinth (Nixon et al., 2016). Lacustrine conditions prevailed during Rift 1, with a transition from episodic marine incursions to periodically fully marine conditions during Rift 2 (~0.6 Ma). This occurred as the Gulf of Corinth opened during interglacial highstands to the Ionian and Aegean seas and into its modern configuration (Freyberg, 1973; Collier, 1990; Collier and Thompson, 1991; Moretti et al.,

2004; Rohais et al., 2007b; Ford et al., 2016; Nixon et al., 2016; Rohais and Moretti, 2017; Gawthorpe et al., 2017a).

Siliciclastic sediments sourced from the Hellenide fold and thrust belt (eroded Mesozoic carbonates, radiolarites and Cenozoic turbidites) were transported northwards and deposited syn-kinematically during Rift phases 1 and 2 (Degnan and Robertson, 1998; Ford et al., 2013; Gawthorpe et al., 2017a). The related stratigraphy is split into three groups in the study area; the Lower, Middle and Upper groups (Ford et al., 2007, 2013, 2016; Rohais et al., 2007a). The Lower Group was deposited during Rift 1, and the Middle and Upper groups during Rift 2. The earliest fluvial and marginal lacustrine deposition occurred from the widespread Kalavrita River system, now preserved in the Lower Group. Subsequently, giant syn-rift fan deltas prograded into the hangingwalls of the major faults: Platanos, Vouraikos, Kerinitis and Selinous (from east to west) in the hangingwall of the P–M Fault, and Evrostini/Ilias to the east of the study area (Figure 2).

The P–M Fault hangingwall deltas constitute the Middle Group, deposited during early Rift 2 (Gawthorpe et al., 2017a). The age of these deltas is constrained to ~1.8 to 0.7 Ma based on pollen analysis at the Vouraikos fan delta (Ford et al., 2007). These syn-rift sediments on the P–M Fault terrace are the target of this study. Previous studies interpret the mudstone–sandstone deposits in Melissia Valley (Figures 2 and 3) as the fluvio-lacustrine Melissia Formation (Backert et al., 2010), constituting part of the older Lower Group (Ford et al., 2007, 2013). These authors describe this succession as being unconformable with overlying fine-grained deposits of the Zoodhochos Formation within the Middle Group, which are interpreted to represent distal turbidites in a bottomset setting (Backert et al., 2010). However, the present study did not observe substantial facies variations between the deposits of the Zoodhochos and Melissia formations, nor was the erosive contact reported by Backert et al. (2010) identified. An alternative interpretation is that all of the fine-grained deposits in Melissia Valley represent fan delta bottomsets to the Selinous and Kerinitis foresets updip (Middle Group), and are equivalent to the Zoodhochos Formation of Backert et al. (2010). Projection of key surfaces within the Selinous foresets into the bottomsets using 3D outcrop models has allowed their correlative foreset packages to be approximately constrained. In addition, the base of the Selinous fan delta axis directly overlies basement rocks; fine-grained fluvio-lacustrine deposits are absent. The Upper Group consists of younger marine terraces and smaller Gilbert-type fan deltas with erosive bases, primarily deposited in the hangingwall of the Helike Fault system (Ford et al., 2007, 2013, 2016; Rohais et al., 2007a).

The focus of this study is the eastern part of the Selinous fan delta and the western part of the Kerinitis fan delta, in the hangingwall of the P–M Fault (Middle Group) (Figures 2C and 3). The Kerinitis fan delta is positioned slightly to the
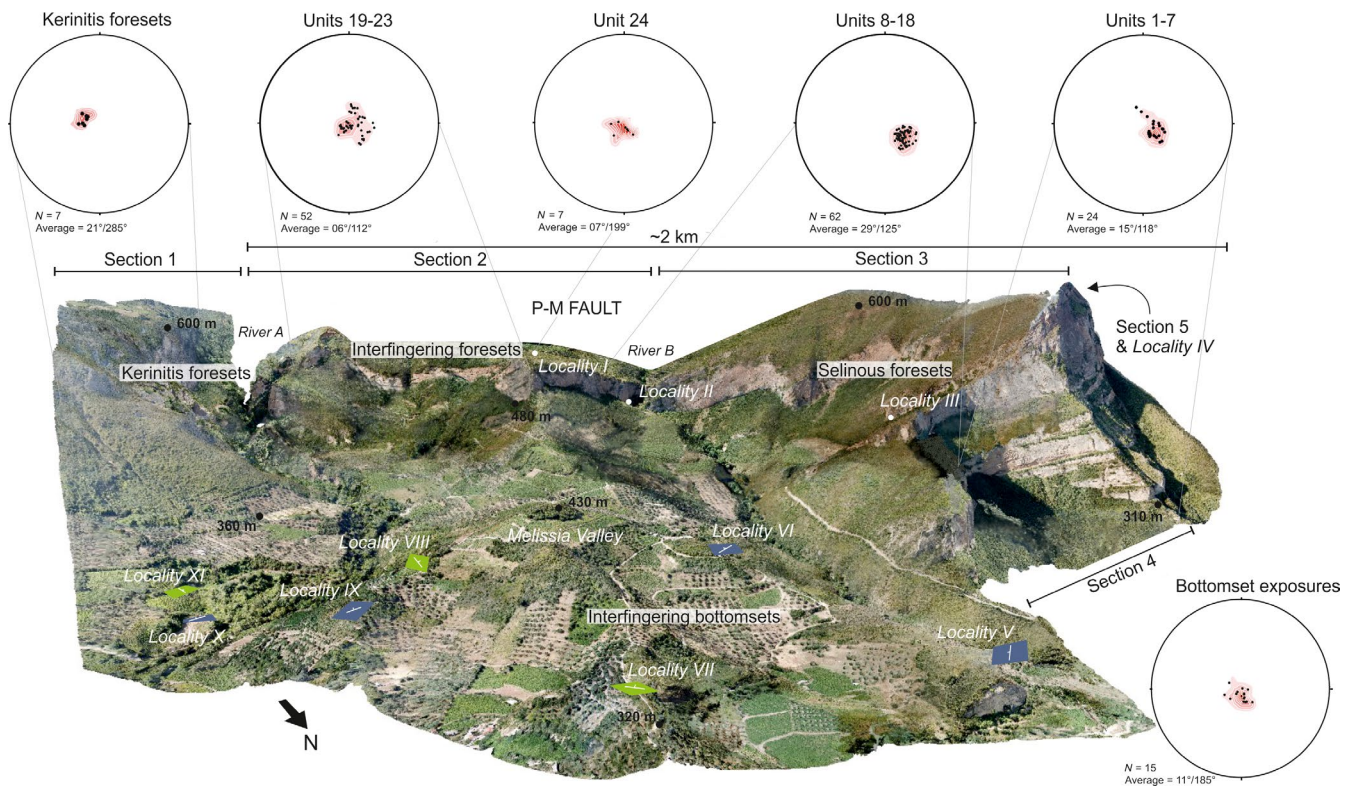
FIGURE 3 Study area and data overview. 3D outcrop model of the interfan study area was created using UAV-photogrammetry data and Agisoft Photoscan software. Stereonets, Sections 1–5, Localities I–XI (bottomset outcrops with coloured planes—created using LIME software) are presented. Green planes represent W-dipping (Kerinitis-derived) outcrops. Blue planes represent E-dipping (Selinous-derived) outcrops. Dip data is taken from the field and from 3D outcrop model structural planes in LIME software and presented with southern hemisphere-projected stereonet plots using Stereonet software. N = number of data points.

west of the P–M fault centre and the Selinous fan delta is positioned ~4 km from the western fault tip. Barrett *et al.* (2019) quantify the minimum period of deposition, average subsidence and sedimentation rates at the Kerinitis and Selinous fan deltas as >451 and 615 kyr, and 0.65 and >1.77 m/kyr, respectively, based upon stratigraphic observations. Numerical modelling was used to quantify the amplitude of climate-induced lake-level changes in Lake Corinth during the Early–Middle Pleistocene at 10–15 m (Barrett *et al.*, 2019). Previous studies focus on the facies and stratigraphic architecture of the axial sections of the Kerinitis and Selinous fan deltas (Dart *et al.*, 1994; Gawthorpe *et al.*, 1994; Backert *et al.*, 2010; Gawthorpe *et al.*, 2017b; Barrett *et al.*, 2019).

The study area consists of a ~300 m high conglomeratic cliff with a ~2 km wide, main north-facing exposure (Sections 1–3; Figures 2C and 3), and additional west (Section 4; Figures 2C and 3) and south-facing (Section 5; Figures 2C and 3) exposures that provide 3D constraints. Section 1 exhibits thick, west-dipping ('W-dipping') units from the Kerinitis fan delta. While these are considered in the interpretation, they are not characterised within the stratigraphic framework due to limited access and difficulty in obtaining reliable UAV-photogrammetric data in that region. The units within Section 2 are generally thinner and stratigraphically

higher than the units in Sections 3–5, and both east-dipping ('E-dipping') and 'W-dipping' units are present with interfingering geometries. This is considered to be the centre of the interfan area. Section 3 consists of several thick 'E-dipping' foreset units from the Selinous fan delta. Section 4 is a curved, generally west-facing section and Section 5 faces SW. Both Sections 4 and 5 consist of 'E-dipping' units. The Old Taxiarches Monastery is built into the Selinous foresets in Section 5. Here, part of the conglomeratic section and a thin, fine-grained interval is accessible (Locality IV; Figures 2C and 3). Otherwise, access to the interfan sections is limited. Associated fine-grained exposures can be found in the valley to the north of the cliff, near Melissia (Localities V–XI; Figures 2C and 3) and represent the fan delta bottomsets.

3 | METHODOLOGY

A DJI Mavic Pro drone was used to collect the photogrammetric data that was augmented by annotated photograph panels and field sketches. Agisoft Photoscan/Metashape and LIME software were used to build and interpret the 3D outcrop models (e.g. Figure 3). Sedimentological and structural data were collected directly in the field where access allowed and

complemented by outcrop model measurements where the exposures were inaccessible. Measured sections of sandstone successions were collected at millimetre to centimetre-scale to document lithology, grain size, sedimentary structures and the nature of bedding contacts. Conglomeratic units were logged at decimetre-scale, with the support of sketches to capture the geometry of large-scale features, such as the continuity of surfaces. Palaeocurrent data were collected from ripple cross laminations, clast imbrication, cross-bed plane measurements and dips of foresets generated from sediment gravity flows. Presented data are unrestored due to the lack of a reliable palaeo-horizontal datum, but the steepest tectonic tilt is ~12° (S).

Figure 4 outlines the methodology for extracting data from 3D outcrop models, which are able to represent measurable objects with a lower limit of ~10 cm. The stratigraphic framework was established from interpretation of the interfan cliff section using LIME software to map stratal surfaces. The 3D outcrop models allowed qualitative (detailed stratal geometries, nature of major surfaces and accurate correlation of surfaces around topography) and quantitative (dip data from bedding planes, stratigraphic thickness, topset-foreset breakpoint trajectories and height of foresets) data collection (Figure 4). In total, 167 bedding dip measurements were collected in the field and using LIME software-based mapping of the 3D outcrop models (Figure 3). Multiple measurements within each unit were taken for averages to be calculated. The data have not been re-oriented in the absence of a reliable palaeo-horizontal datum. Bedding data collected from the outcrop models were validated against field measurements at the Old Taxiarches Monastery (Figure 2). The east and west components of dip are used to differentiate between beds or units from the Selinous and Kerinitis fan delta systems, respectively.

Bedding measurements often have north or south dip components as well, but as both fan deltas prograde northward and both are back-tilted to the south towards the P–M fault, the east and west components are the most useful diagnostic criteria.

Correlation of surfaces around topography and constraining the stratigraphic position of associated bottom-set outcrops in the valley were refined with the use of 3D outcrop models. By projecting planes following the dip of the foresets in Sections 3 and 4 into Melissia Valley, the E-dipping (Selinous) fine-grained, bottomset outcrops could be correlated to their updip foreset counterparts in the interfan area. A typical clinoform profile shallows in dip at the foreset-bottomset transition. Therefore, the constant dip of the projected foreset planes mean that the units assigned to bottomset deposits are approximate, but are more likely to be associated with lower units than higher units. Where the bottomset outcrops are W-dipping, they are derived from the Kerinitis fan delta and cannot be tied updip, but instead their relative position to Selinous units is recorded.

4 | RESULTS

4.1 | K–S facies association characterisation

Eight facies associations (FAs) characterise the Selinous and Kerinitis fan deltas, based on geometric position (topset–bottom-set) and depositional environment (Table 1; Figures 5 through 7). The main fan delta units are constructed from conglomeratic, fluvial and shallow water topset and foreset facies associations (FA 1a–b; 2a–b; 3). The facies associations observed in the interfan area are the focus: the foreset facies association
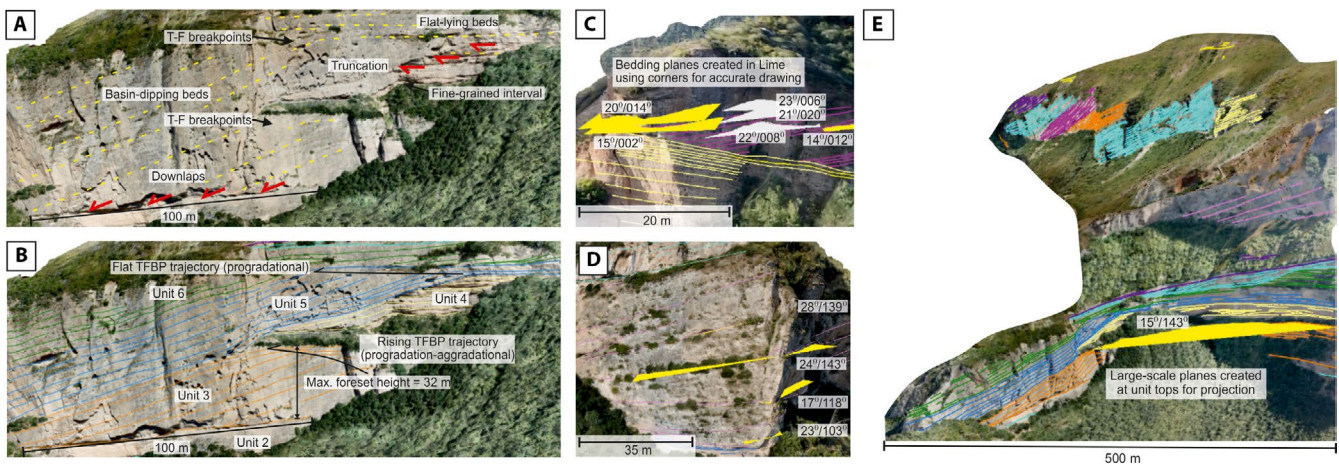

FIGURE 4 Methodology for stratigraphic architecture interpretation and for obtaining quantitative information from UAV photogrammetry-based 3D digital outcrop models. (A) observations from part of Section 4, where remnants of fine-grained intervals, truncation and clear stratal termination geometries allow units to be divided and contacts to be classified. Topset-foreset breakpoints (TFBPs) can be identified. (B) Interpretation of section shown in (A) with TFBP trajectories and foreset heights indicated. (C and D) Demonstrations of obtaining accurate dip data (convention: dip/dip direction) from small-scale bedding planes (assured using field data) in parts of Section 2. (E) Large-scale planes from unit tops are created and used for projecting across valleys to assist correlations and constraining the stratigraphic position of bottomset outcrops (Sections 3 and 4). 3D outcrop models created in Agisoft Photoscan and interpreted in LIME software.

TABLE 1 Facies associations at the Selinous and Kerinitis fan deltas (modified from Barrett *et al.*, 2018). See Supporting information for facies information.

FA code	Constituent facies	FA interpretation	Sub-association
1a	Co1, Co2	Fluvial topset	Channel-fill
1b	Co1, Sa2, Sa6, Fi3		Delta plain
2a	Co4, Co5	Shallow water topset	Beach barrier
2b	Co1, Co4, Co5, Co7, Sa1, Sa2 and Sa4		Upper shoreface
2c	Co5		Lower shoreface
3	Co3, Co4, Sa4	Foreset	
4a	Sa1-6, Fi1-2, Fi4-8	Bottomset	Deep-water
4b	Co6, Sa1-6, Fi1, Fi2		Shallow-water

that occupies the majority of the interfan cliff sections (FA 3), and the bottomset facies associations that are found in Melissia Valley, and in the Unit 8-9 fine-grained interval/flooding surface (FA 4a). An additional facies association to the scheme of Barrett *et al.* (2019) is FA 2c (upper shoreface, which occurs in the shallow water topset; Locality I; Figure2; Table 1). Four facies (Supporting information) have been added to the bottomset facies association of Barrett *et al.* (2019).

4.1.1 | FA 1: Fluvial topsets

Two fluvial topset facies associations are identified from the fan delta axes: FA 1a) channel-fill, and FA 1b) delta plain depositional environments. Channel-fill (FA 1a) is the most common and comprises poorly-sorted, sub-angular to sub-rounded, sandy gravel-cobble conglomerate with clast imbrication and erosive bed bases. These deposits are interpreted to represent bedload deposits during high energy fluvial flow regime. The delta plain FA 1b comprises poorly-sorted, sub-angular, sandy gravel-cobble conglomerates interbedded with normally graded, gravelly-coarse sand beds. Red palaeosols (centimetre-thick) are found between gravelly coarse sandstone beds (Barrett *et al.*, 2019). A variable, periodic flow regime is envisaged, with periods of subaerial exposure indicative of overbank deposits in a delta plain environment.

4.1.2 | FA 2: Shallow water topsets

The shallow water topset (FA 2) is divided into three sub-associations: 2a) beach barrier, 2b) upper shoreface, and 2c) lower shoreface. Only the upper shoreface (FA 2b) is observed in the interfan area, during the latest stage. The beach barrier (FA 2a) consists of a mounded body and internal bi-directional metre-scale cross-beds, with well-sorted, open-framework and mainly rounded pebbles. This indicates textural maturity and character typical of beach reworking. The lower shoreface FA 2c comprises metre-scale, bi-directional, asymptotic cross-beds resembling hummocky-cross stratification (Barrett *et al.*, 2019). These deposits are characteristic of storm reworking below fair weather wave base.

The upper shoreface (FA 2b) is identified in the interfan area (Locality I, Section 2, Figure 2; logs and photographs in Figure 5). Locality I is situated 650–800 m from the fault and the FA 2b are the highest and youngest rocks encountered. Figure 5 presents representative logs and photographs of two of the exposures; one where cross-beds dip eastward and are part of the Selinous fan delta, and one where cross-beds dip westward and are part of the Kerinitis fan delta. Despite opposing bedding dips between the various outcrops at Locality I, the facies are similar, comprising interbedded fine sand to pebble conglomerate (decimetre-scale) beds, between thicker (metre-scale) and coarser grained conglomerates at the bases and tops. Several pebbly gravel beds pinch out laterally over 1–2 m with slight convex-up geometries. These bedforms generally have erosive bases and are matrix and clast-supported, with sub-angular to rounded clasts. Beds are well-sorted, either normally or inversely graded and sands contain gravel and pebble clasts. The thicker conglomeratic beds generally coarsen upwards (sometimes normally-graded) and are poorly-sorted, mostly clast-supported, pebble-cobble grade with sub-rounded to rounded clasts (<18 cm). Clasts are imbricated following the bedding dip (e.g. log 2; Figure 5).

These deposits are interpreted to represent a variable, but generally high energy regime. The lack of fine-grained sediment, and the observed lenticular geometry of the beds, maturity of the clasts and spatial context within a flat-lying unit, suggests reworking of material in the interfan topset area and bedform migration by wave-related currents. The sediments are interpreted to have been deposited in an upper shoreface environment with longshore transport as the main depositional process. Similar processes are observed at the modern Selinous and Meganitis fan deltas in the Gulf of Corinth, as sediments are reworked with the prevailing westerly wind/ wave direction into interfan embayments (Figure 2A).

4.1.3 | FA 3: Foresets

The foreset facies association was described previously by Backert *et al.* (2010) and Barrett *et al.* (2019) and occupies most of the interfan cliff section. It comprises well to

poorly-sorted, clast-supported and open-framework, sub-rounded, mainly pebble-cobble conglomerates. Scours and inverse grading are common. Any matrix is sand-gravel grade, and locally clasts are imbricated. Foresets comprise steep, basinward-dipping (22–25°) beds with heights ranging from ten to a few hundred metres, dependent on palaeo-water depth (and subsequent erosion). The processes responsible are interpreted to be dominated by sediment gravity flows (conglomerate-rich inertial grain flows to non-cohesive debris flows) on the delta foresets (Postma, 1984; Nemec, 1990; Orton and Reading, 1993; Sohn *et al.*, 1997; Sohn, 2000; Rohais *et al.*, 2008; Gobo *et al.*, 2015). In the interfan, the foresets are accessible and described at Localities II and III on Section 3 and Locality IV on Section 5 (Figures 2C and 3).

4.1.4 | FA 4: Bottomsets

Bottomset deposits occur in relatively shallow water when delta clinothems build out over a previous fan delta topset following a transgression (shallow water bottomsets) and in deeper water, basinward of the foreset slope, when it builds past the topset-foreset breakpoint (deep water bottomsets). The interfan bottomset deposits here are characterised within this scheme and provide further insight into the processes at the toe of the foreset slope in interfan areas.

Within both shallow and deep bottomset facies associations, pebble-cobble horizons are present within fine-grained sections, representing sediment gravity flows or rock falls. In other cases, thicker beds are present that comprise poorly-sorted, matrix-supported (fine-coarse sand), graded, gravel-boulder conglomerates with erosive and/or loaded bases and occasional injectites in the underlying beds (Figure 6). These deposits are interpreted as debrites sourced from the delta foresets.

FA 4a: Deep water bottomsets
Deep water bottomsets (FA 4a) comprise interbedded sandstones and calcareous mudstones (FA 4a and 4b in Barrett *et al.*, 2019). Soft sediment deformation features, such as convolute laminations at the upper contact with overlying conglomerates are common. At the fan delta axes, the sandstones contain wavy laminations, inverse grading, slightly erosive bases and localised gravel lags (Backert *et al.*, 2010; Barrett *et al.*, 2019). In the interfan area, the more extensive and thicker exposures allow this FA to be characterised further. Representative logs and photographs are presented in Figure 6. Locally, thin, current-ripple laminated sandstones are draped by black organic material (e.g. Locality X; Figure 6), or intercalated with decimetre-scale, organic-rich mudstone-siltstone beds (e.g. Locality VIII; Figure 6). Thicker, normally graded sandstone beds (~5 to 10 cm) with planar and wavy-laminations, gravel and mudstone clasts, and broken and whole brachiopod shells (<2 cm diameter) are common.

Much like the fan delta axes, the conglomeratic interfan succession is punctuated by thin (<2 m), fine-grained intervals. The only fine-grained interval that is accessible in the interfan area is exposed in Section 5 (Locality IV), within the Old Taxiarches Monastery (Figure 7). The section comprises a coarsening-upwards succession of mudstone to gravel, overlain by an erosional ~1 m thick, poorly sorted, clast-supported gravel-cobble conglomerate (mainly large pebble) with sub-rounded to sub-angular clasts. The mudstone-siltstones at the base of the section are planar and wavy laminated. There are two thin, normally graded sandstones before a dark, organic-rich silty mudstone. The mudstone is overlain by lower medium sandstone (0.8–0.9 m) containing gravel and broken shell lenses (gravelly-coarse sand matrix) with evidence for soft sediment deformation (Figure 7). The interval is positioned basinward of the topset-foreset breakpoint and between two units of high (>100 m), steeply-dipping foresets, suggesting a relatively deep water position that is below wave base, even allowing for changes in base level.

The sandstones are interpreted to be turbidites, with finer-grained beds representing quiet periods between events, or dilute turbidity currents. Some outcrops have a narrow palaeo-current dispersal pattern (e.g. Locality VIII, Figure 6), which implies the deposits are inherited from a single system. Others have multiple palaeocurrent directions between beds (e.g. Locality X, Figure 6) implying both Kerinitis and Selinous fan delta sources (Figure 6). In addition, a number of palaeocurrent measurements have a southerly component, opposite to the regional trend, which could indicate flow reflection and deflection from local topography (Potter and Pettijohn, 1977; Kneller *et al.*, 1991; Lomas and Joseph, 2004; Bell *et al.*, 2018).

FA 4b: Shallow water bottomsets
Barrett *et al.* (2019) previously classified the shallow water bottomset (FA 4b) as coarse (sand to gravel-grade) sediments with multiple and diverse sedimentary structures, such as symmetrical and asymmetrical ripple laminations, wavy and planar laminations, dune-scale gravel cross-beds and soft-sediment deformation, indicating sediment gravity flows and wave re-working operating at the base of slope in shallow water. This facies association is identified at the fan delta axis (Barrett *et al.*, 2019), but not in the interfan area. Some bottomset deposits are observed in Section 2 of the interfan area (Figure 8) at the down-dip termination of relatively short foresets that could exhibit FA 4b, but it is not possible to access them to constrain the facies.

4.2 | Stratigraphic architecture

4.2.1 | Key stratal surfaces

Key surfaces were identified in the field and 3D outcrop models, and are used to subdivide the interfan succession into stratal units associated with both the Selinous and Kerinitis fan deltas. Key surfaces are recognised based on the presence
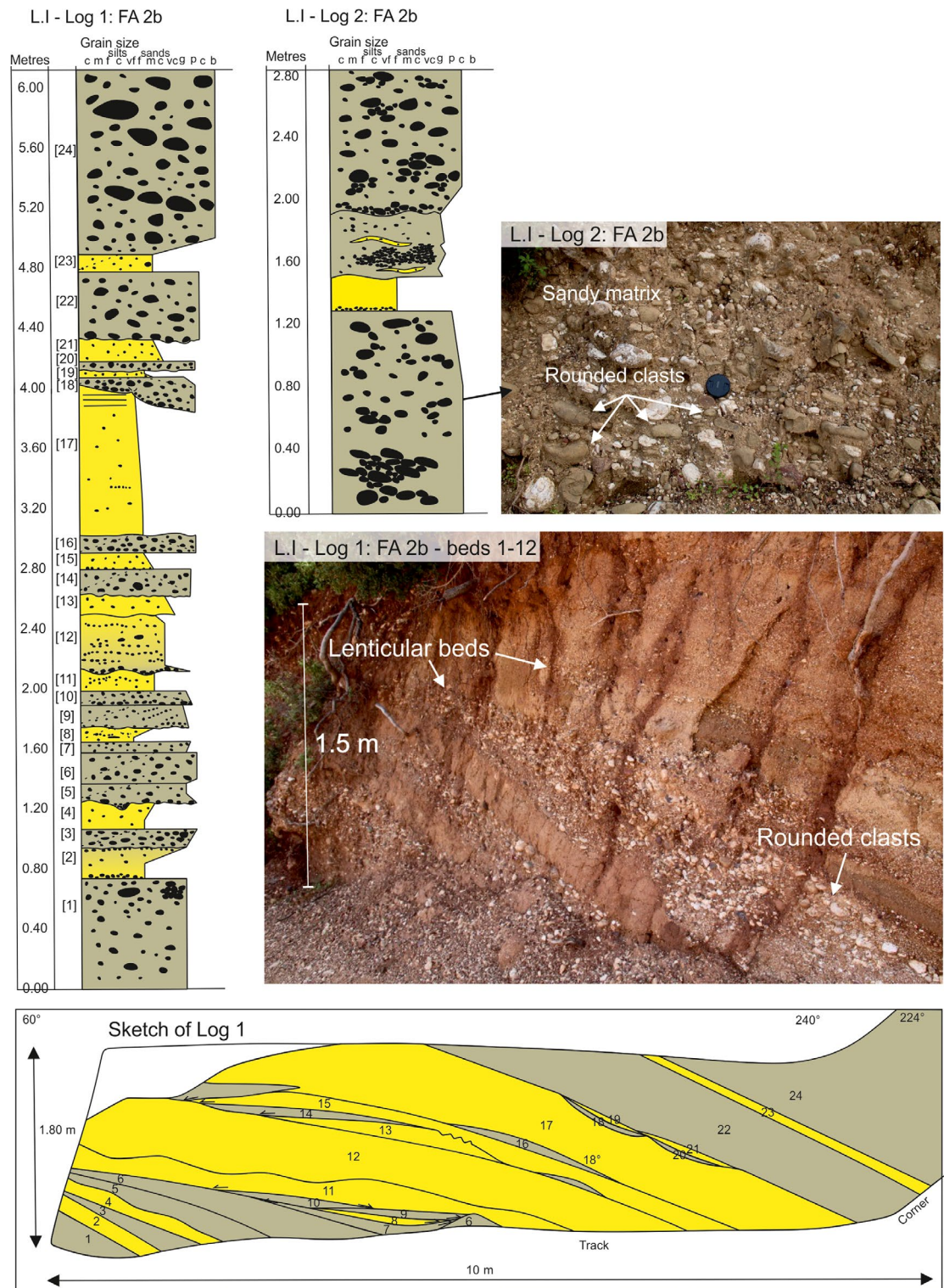
FIGURE 5 Shallow water topset—upper shoreface facies association (FA 2b). Logs 1 and 2 and associated photographs show two representative outcrops from Locality I. The bracketed numbers on Log 1 correspond to the numbered beds on the outcrop sketch. Yellow = sandstone; grey = conglomerate. Log 1 and Log 2 outcrops have an average bed dip/dip direction of 17°/270° (Kerinitis-derived) and 05°/160° (Selinous-derived), respectively.

of fine-grained deposits, deeply erosional surfaces and/or evidence of onlap, downlap, offlap or truncated stratal relationships. Fine-grained intervals (<2 m thick) are apparent between the delta topsets, with some remnants between foreset units, both in the fan axes and in the interfan area. The interpretation of each surface is described as either confident or uncertain.
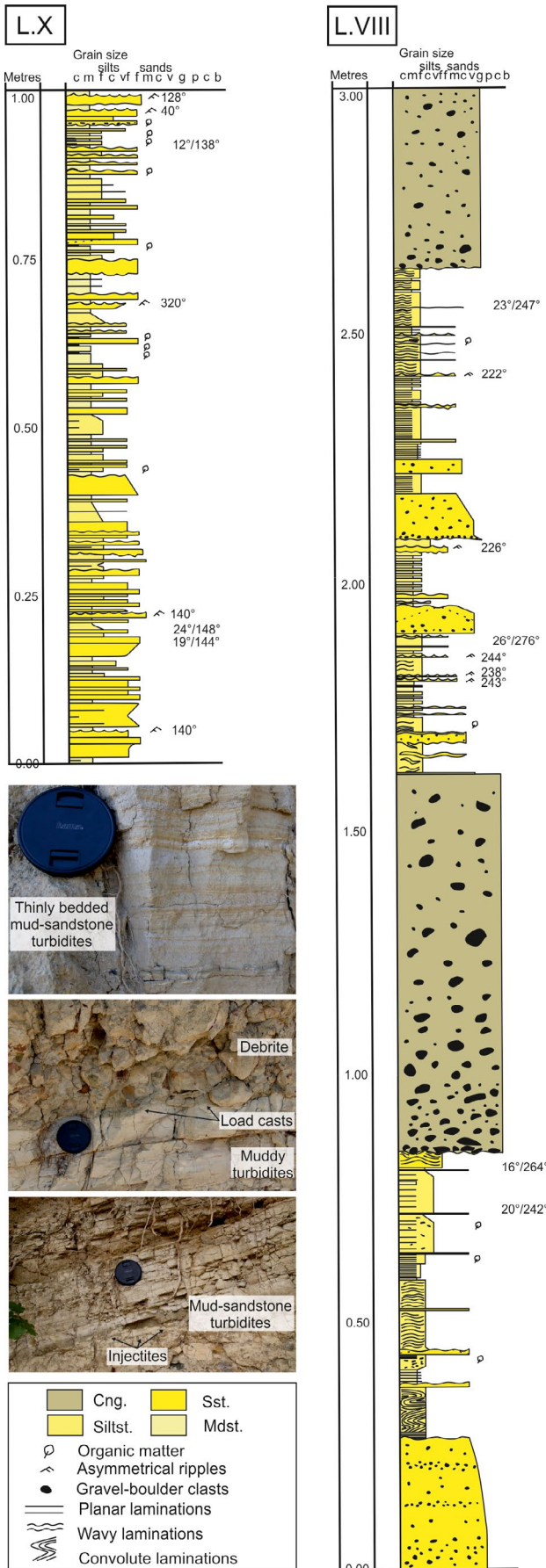
FIGURE 6 Representative bottomset logs from Localities L.X and L.VIII (Figures 2C and 4) in Melissia Valley (FA 4a). Mudstone-sandstone turbiditic successions with occasional debrites are shown. The sandstone-mudstone content is variable between them. Palaeocurrent directions suggest input from both Kerinitis and Selinous systems and in some cases with a southerly component, suggesting redirection from local topography. Photographs illustrate some of the features in the logs. Cng = conglomerate, Sst = sandstone, Siltst. = siltstone, Mdst = mudstone.

The nature of each surface is described in Table 2 and examples from Section 2 are presented in Figure 8. Units 1–9 (Section 4; Figures 2C and 9) and 13–15 (Section 3; Figures 2C and 9) have top contacts that have been identified confidently as key surfaces. The top of Unit 1 is a major downlap surface (Unit 15). Fine-grained intervals are preserved in places at the tops of Units 2, 3, 8 and 13–15, despite their position in the dynamic foreset region where fine-grained material has a low preservation potential. Units 3–5 have topset-foreset breakpoint trajectories exposed, suggesting a transitional position between delta topsets and foresets, but generally the interfan is characterised by steeply-dipping, foreset units. Erosive surfaces that clearly truncate underlying foresets are present at the tops of Units 4, 6 and 7. The interpretation of the top contacts of Units 10–12 and 16 are uncertain. Units 17–22 have confident key surfaces identified at their tops. Surfaces at the tops of Units 17–19 are erosive and fine-grained intervals are preserved. Erosional surfaces are more pervasive towards the top of the section and fine-grained intervals are not present between the upper units (20–22). The tops of Units 23 and 24 are not exposed.

4.2.2 | Key stratal surface interpretation

The base of each fine-grained interval is interpreted to represent a transgressive surface, although the lateral extent of the surfaces is unknown. Fine-grained intervals are present between units in all of the fan deltas in the hangingwall of the P-M Fault, but due to lack of age constraint it is not possible to correlate the surfaces. Between Units 8–9, an organic-rich silty mudstone bed separates graded sandstones in a generally coarsening-upward, mudstone to gravel sequence. This could be interpreted to contain a maximum flooding surface, but the regional continuity of the surface is unknown. The surface is overlain by storm reworked shallow marine deposits (overlying broken shell fragments in gravelly sand lenses) and turbidites, likely associated with the progradation of the subsequent foreset unit.

In the topsets, abrupt shifts in depositional environment are apparent from facies changes and evidence of subaerial exposure. Deep erosion surfaces overlain by palaeosols are interpreted to occur as a result of relative base-level fall,

but cannot be correlated across adjacent fan deltas. In the foreset to bottomset regions, as with the interfan, base-level changes and stratigraphic surfaces can be expressed differently to topset axial regions. Lack of subaerial exposure and significant environmental shift during relative base-level fall mean that major sediment bypass zones (Stevenson *et al.*, 2015) are candidate sequence boundaries. However, erosive events are not only triggered by relative base-level fall, particularly in seismically-active regions. As such, sequence boundaries can either be masked or simply misinterpreted—a common problem in deep water successions (Covault and Graham, 2010; Hodgson *et al.*, 2016). Where foresets overlie fine-grained prodelta deposits, there are often erosive contacts ('cuspate' erosion surfaces at the Kerinitis fan delta axis; Backert *et al.*, 2010), which could be slide scars or scour surfaces. Unlike the Selinous fan delta, subaerial unconformities are absent at Kerinitis, because the rate of accommodation increase exceeded the rate of base-level fall at the fault centre (Gawthorpe *et al.*, 1994; Hardy and Gawthorpe, 1998; Backert *et al.*, 2010; Barrett *et al.*, 2019).

The base-level changes are attributed to changes in lake level (~10 to 15 m; Barrett *et al.*, 2019) in response to climate variations that followed 41 kyr orbital cycles. This cyclicity is documented in Greece and the Mediterranean (Capraro *et al.*, 2005; Dodonov, 2005; Suc and Popescu, 2005) and globally during the Early–Middle Pleistocene (Emiliani, 1978; Head and Gibbard, 2005; Lisiecki and Raymo, 2007). There is some evidence of episodic marine flooding, as global sea-level rise opened Lake Corinth to the Ionian Sea and Aegean Sea during interglacial highstands (Freyberg, 1973; Collier, 1990; Moretti *et al.*, 2004; Rohais *et al.*, 2007b, 2008). Overall, relative base-level changes were superimposed onto a lower frequency, background tectonic regime, initially dominated by high subsidence rates on the P–M Fault, and later by uplift from the West Helike Fault. A variable sedimentation rate is also likely influenced by climate-driven fluctuations in sediment supply (Collier, 1990; Collier *et al.*, 2000).

4.2.3 | Major unit sets

The fan delta stratigraphy is generally made up of topset or foreset conglomerate beds (10s m thick), separated by thinner (<2 m), finer-grained mudstone-sandstone intervals. Twenty-four stratal units are identified in the interfan area, comprising both E-dipping (Selinous-derived) and W-dipping (Kerinitis-derived) beds. These units are separated by the key stratal surfaces described above. Considering only the key surfaces interpreted confidently, there are a minimum of 20 units. At the fan delta axes, 15 units are identified at the Selinous fan delta (Barrett *et al.*, 2019), and 11 are identified at the Kerinitis fan delta, although the base of the Kerinitis fan delta is not exposed (Backert *et al.*, 2010). Successive units that share characteristics are compiled into unit sets. The common characteristics are progradation direction and/or relative geometrical position. Units and unit sets are defined based on observations and may or may not have sequence stratigraphic significance; they do not imply a particular position within a depositional sequence. Observations
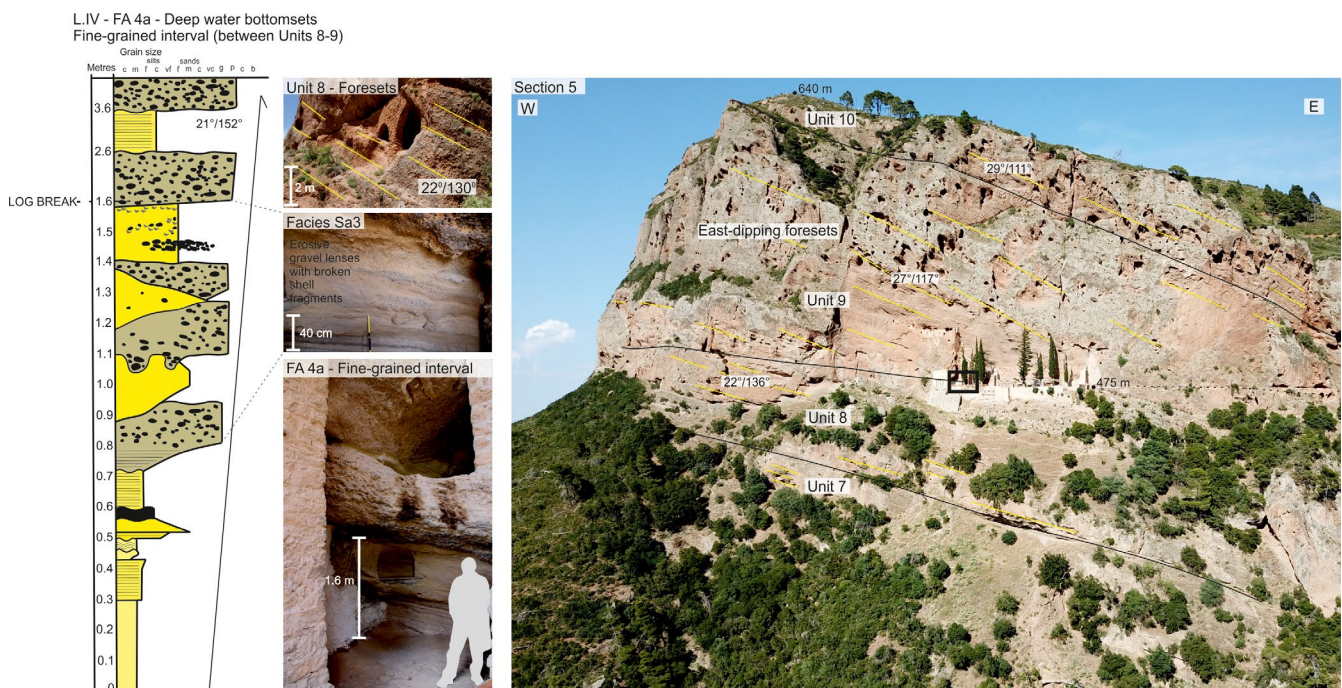

FIGURE 7 Section 5 and Unit 8 and 9 fine-grained interval character at Locality IV. Photographs of foreset facies association (FA 3). Log and photographs of distal bottomset facies association (FA 4a) and facies Sa3 (Supporting information) therein.
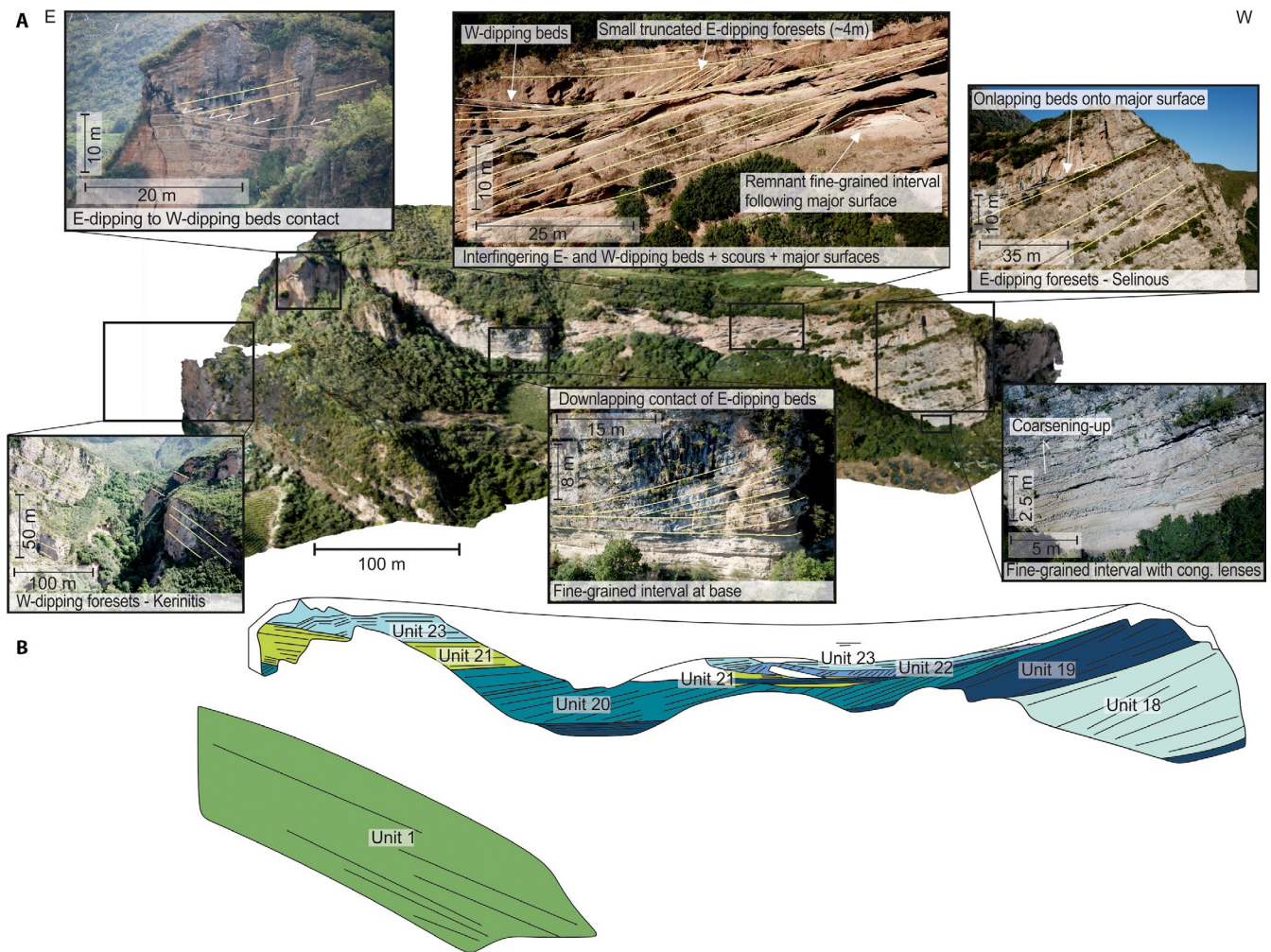
FIGURE 8 (A) Key stratigraphic observations of Section 2. E-dipping beds are Selinous-derived and W-dipping beds are Kerinitis-derived. (B) Stratigraphic framework of the central interfan face—Units 18-23 (Section 2). 3D outcrop model created in Agisoft Photoscan.

and the stratigraphic framework of Section 2 are presented in Figure 8. The stratigraphic framework for the whole interfan (Sections 2–4) is presented in Figure 9. Table 2 summarises data derived from each unit. Bedding data are presented with dip and dip direction (Figure 3).

The surfaces from the interfan cannot be accurately correlated to those at the Selinous and Kerinitis axes due to accessibility, outcrop continuity across river valleys and the absence of chronostratigraphic data. However, it is assumed that all units expressed at the Selinous fan delta axis (15 units) are observed in the interfan area (20 Selinous-derived units). Unit 1 in the interfan is part of the Kerinitis fan delta and can be traced updip to sit within the middle of the Kerinitis axial stratigraphy. The foresets markedly thicken and become higher in Units 9 and 10 at both the axis of Selinous (Barrett *et al.*, 2019) and in the interfan stratigraphy, so the lower stratigraphy in the interfan (Units 2–16) is tentatively correlated to the axial Selinous units (Figure 10). Correlations of the bottomset deposits in Melissia Valley were attempted using the 3D outcrop

models, but these remain uncertain given the limited continuity of the outcrop.

Unit set 1
Unit set 1 only comprises Unit 1, a foreset unit (FA 3) with average foreset dips of 20° towards 345°, which suggests it is part of the Kerinitis fan delta. The unit is at least 60 m thick, although the base is not observed. In Section 3, the top is downlapped by E-dipping beds of Unit 15 (Figure 9). It is not possible to tie this unit directly to the stratigraphic framework of the Kerinitis axis, but it sits somewhere within the middle units of Kerinitis. Bottomsets at Locality VII (FA 4b; Figure 3) also dip westward, supporting a Kerinitis fan delta origin. The outcrop is positioned between planes projected from the top of Unit 2 and top of Unit 3 Selinous foresets. However, these planes have a constant dip and likely overestimate bedding dip. This, combined with the absence of W-dipping foresets associated with Unit set 2, indicates that these bottomsets are likely to be associated with Unit 1.

TABLE 2 Stratigraphic information of the units in the K–S interfan area.

Unit	Observed position of unit	Average dip/dip dir.	Nature of basal contact	Top contact interp.	Fine-grained interval at top? (Y/N)	Nature of top contact	Observation type for contacts	Stratigraphic thickness	Foreset height	T-F breakpoint apparent? (Y/N)	T-F breakpoint trajectory
1	Sections 2 and 3	20°/345°	Not exposed	Confident	N	Downlapped by overlying, E-dipping beds	Multiple 2D	>60 m	>100 m	N	
2	Section 4	12°/140°	Not exposed	Confident	Y	Conformable contact with thin (<2 m) fine-grained interval at top	2D	>18 m; Max. preserved 35 m		N	
3	Section 4	14°/074°; 15°/143°	Slightly erosive contact with downlapping beds onto the fine-grained interval between Units 2 and 3	Confident	Y	Conformable contact with thin (<2 m) fine-grained interval at top	2D	33 m	32 m	Y	Progradation-aggradation
4	Section 4	15°/075°; 15°/150°	Erosive contact with fine-grained interval	Confident	N	Erosive	2D	16 m	>8 m	Y	Aggradation
5	Section 4	17°/088°; 17°/146°	Erosive contact in NE-dipping region and conformable in SE-dipping region	Confident	N	Conformable contact with Unit 6	2D	8–22 m	>45 m	Y	Progradation
6	Section 4	25°/104°	Conformable	Confident	Y	Erosive	2D	Max. preserved 25 m	>45 m	N	
7	Section 4	26°/133°	Erosive	Confident	N	Slightly erosive		<23 m		N	
8	Sections 4 and 5	22°/136°	Erosive	Confident	Y	Conformable contact with thin (<2 m) fine-grained interval at top	Multiple 2D	~35 m		N	
9	Section 4 and 5	27°/117°	Slightly erosive contact with fine-grained interval	Confident	N	Poorly imaged at top of outcrop model	Multiple 2D	90 m	>50 m	N	
10	Section 3	29°/111°	Appears conformable in western section	Uncertain	N	Poorly exposed	2D	<80 m	>100 m	N	
11	Section 3	34°/140°	Poorly exposed	Uncertain	N	Dip and geomorphological change	2D	~60 m	>100 m	N	
12	Section 3	36°/111°	Dip and geomorphological change	Uncertain	N	Geomorphological surface—cut back into cliff	2D	~65 m	>90 m	N	
13	Section 3	38°/135°	Geomorphological surface—cut back into cliff	Confident	Y	Conformable contact with fine-grained interval	2D	~43 m	>90 m	N	
14	Section 3	37°/125°	Erosive	Confident	Y	Conformable contact with fine-grained interval	2D	~30 m	>80 m	N	

(Continues)

TABLE 2 (Continued)

| Unit	Observed position of unit	Average dip/dip dir.	Nature of basal contact	Top contact interp.	Fine-grained interval at top? (Y/N)	Nature of top contact	Observation type for contacts	Stratigraphic thickness	Foreset height	T-F breakpoint apparent? (Y/N)	T-F breakpoint trajectory
15	Section 3	31°/111°	Slightly erosive	Confident	Y	Conformable contact with fine-grained interval	2D	~40 m	>50 m	N	
16	Section 2 and 3	27°/123°	Conformable	Uncertain	N	Conformable	Multiple 2D	~30 m	>50 m	N	
17	Section 2	26°/134°	Conformable	Confident	Y	Erosive and fine-grained interval present	2D	~65 m	>50 m	N	
18	Section 2	24°/125°	Erosive in places and coarsens up from underlying fine-grained interval	Confident	Y	Slightly erosive and remnants of fine-grained interval	2D	~58 m	>50 m	N	
19	Section 2	26°/127°	Slightly erosive and remnants of a fine-grained interval	Confident	Y	Erosive and fine-grained interval present	2D	~27 m	>40 m	N	
20	Section 2	16°/073°	Downlaps underlying erosive surface and fine-grained interval	Confident	N	Erosive	2D	16–26 m	>25 m	N	
21	Section 2	12°/247°; 09°/196°; 08°/231°, 14°/133°, 14°/236°	Erosive	Confident	N	Conformable	2D	7–16 m		N	
22	Section 2	28°/148°	Downlapping Unit 21	Confident	N	Erosive	2D	<4–5 m	>4 m	N	
23	Section 2	19°/015°	Truncates Unit 22 in central part and downlaps Unit 21 in eastern part	Uncertain	Not exposed	Not exposed	2D	>18 m		N	
24	Section 3	15°/113°	Not exposed	Not exposed	Not exposed	Not exposed	2D	>20 m		N	
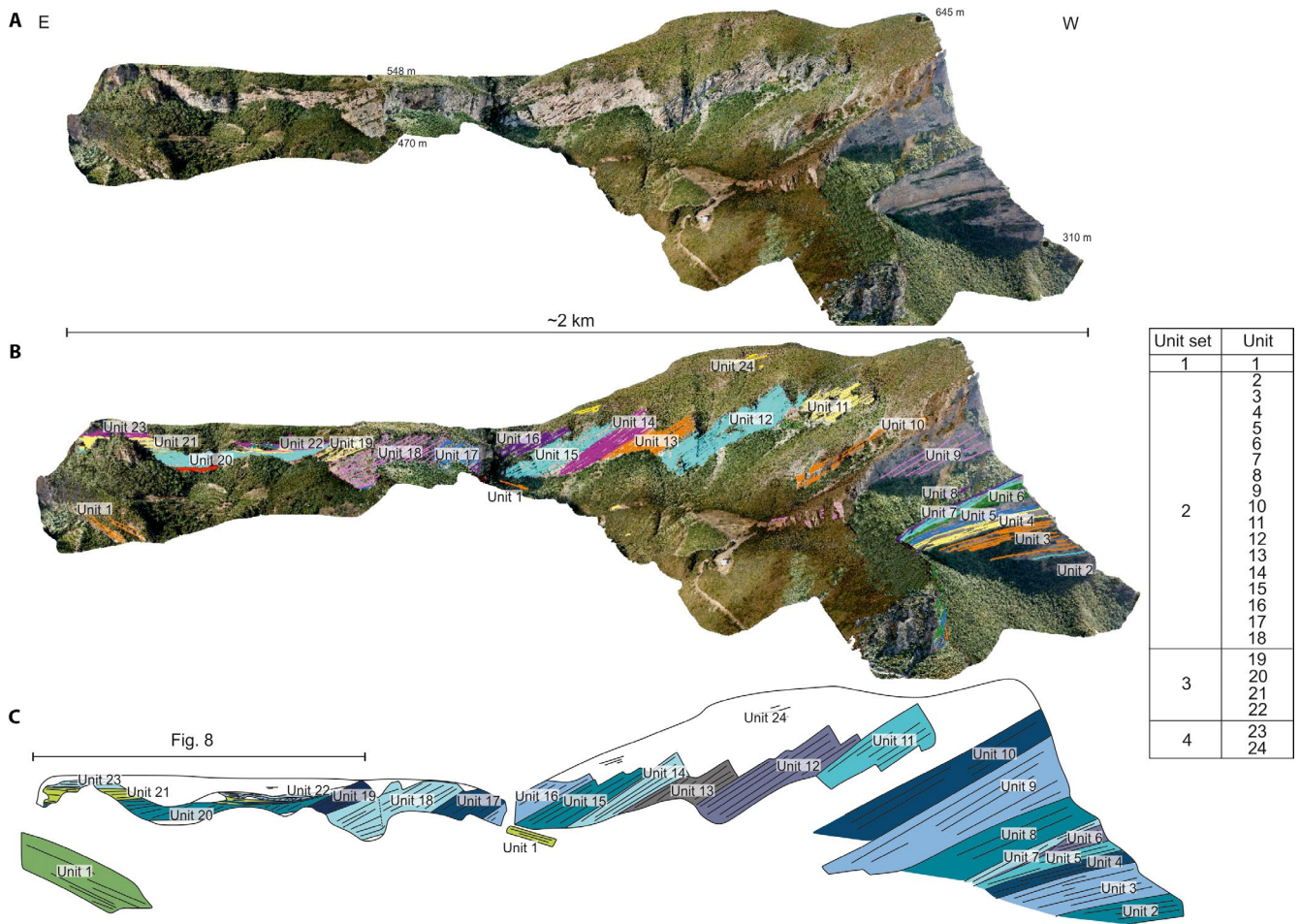
FIGURE 9 Stratigraphic framework of entire north-facing interfan cliff section (Sections 2–4). (A) Clean 3D outcrop model. (B) Interpreted 3D outcrop model with stratigraphic framework—Units 1-24. (C) Schematic cross-section of stratigraphic framework. Blues indicate units from Selinous; green indicates units from Kerinitis. 3D outcrop models are UAV-photogrammetry based, built in Agisoft Photoscan and interpreted with LIME software. Inset table shows the corresponding units within the four unit sets.
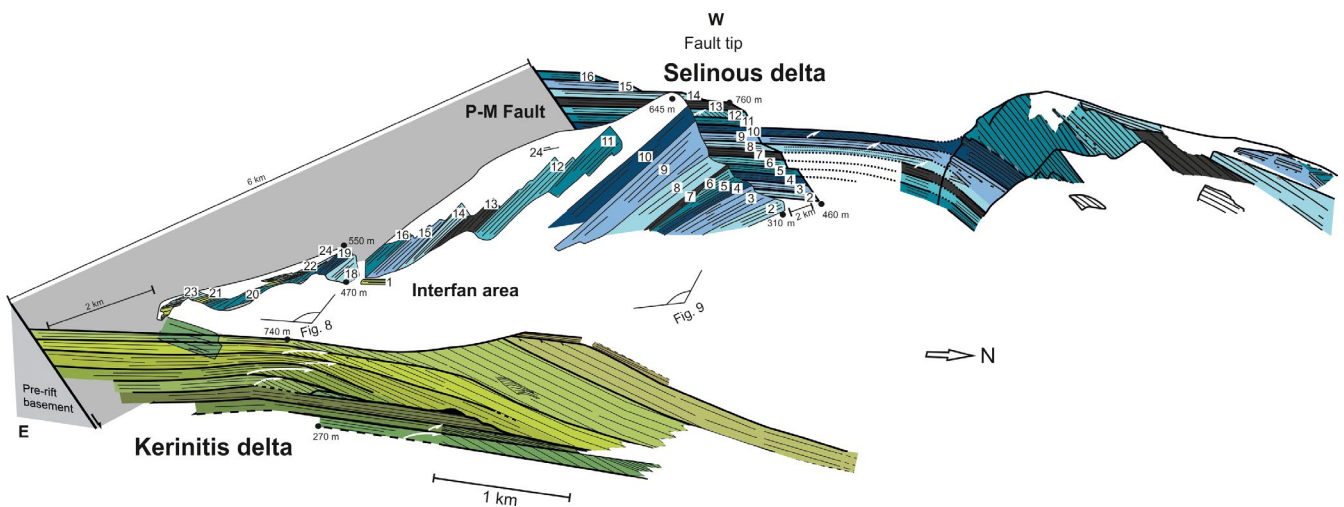
FIGURE 10 Summary diagram of stratigraphic architecture of Kerinitis (green units) and Selinous (blue units) fan deltas. Two dip sections are presented (modified from Barrett et al., 2018). An along-strike section from this study showing interfingering of the two systems in the interfan area is added to show both down-dip and along-strike stratigraphic architecture. White arrows indicate topset-foreset breakpoint trajectories. Numbers correspond to unit numbers from this study. Correlative topset units are numbered at the Selinous fan delta axis, but do not correspond to unit numbers in Barrett et al. (2018).
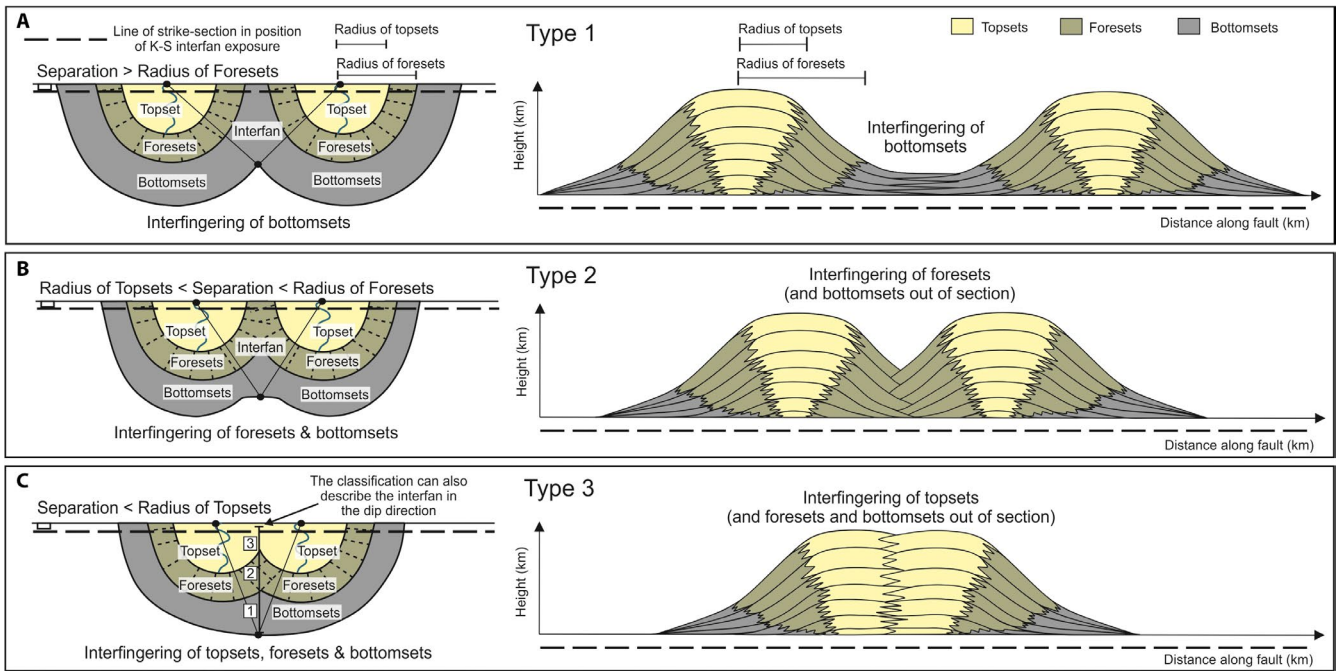
FIGURE 11 Interfan classification scheme, Types 1-3 in plan view and strike cross-section. (A) Type 1—two adjacent fan deltas are separated by a distance > foreset radius and only the bottomsets interfinger in the interfan. (B) Type 2—two adjacent fan deltas are separated by a distance > topset radius and < foreset radius, and foresets and bottomsets interfinger in the interfan. (C) Type 3—two adjacent fan deltas are separated by a distance < topset radius, and topsets, foresets and bottomsets interfinger in the interfan.

Unit set 2

Units 2–18 comprise Unit set 2, and all have eastward bedding dips (average 27° towards 122°) indicating they are part of the Selinous fan delta (Figures 3 and 9). According to projected planes in the 3D outcrop model, the bottomset outcrop at Locality V in Melissia Valley (FA 4b; position in Figure 3) is E-dipping and positioned between the top of Unit 1 and the top of Unit 2, and is therefore assigned to Unit 2.

Topset-foreset breakpoints are apparent in the lower Units 3–5 (Figure 4). Within Unit 3, the topset-foreset breakpoint presents a progradational–aggradational trajectory. Beds are observed that dip to the NE (14° towards 074°) and SE (15° towards 143°) revealing the radial pattern of the fan delta. The NE-dipping beds downlap the fine-grained interval below, and the SE-dipping beds project into the outcrop face. The maximum height of the NE-dipping foresets from topset-foreset breakpoint to the downlap position is 32 m (Figure 4). A thin, fine-grained interval overlies Unit 3, which is eroded by Unit 4. The topset-foreset breakpoint of Unit 4 is observed above that of Unit 3 and has an aggradational (near vertical) trajectory. Beds dip to the NE (15° towards 075°) and SE (15° towards 150°). The height of the youngest foreset before Unit 5 is 8 m. The upper part of Unit 4, with NE-dipping beds, is eroded by Unit 5. The topset-foreset breakpoint of Unit 5 reveals a near-horizontal, that is, progradational, trajectory (Figure 4). The beds dip eastward (15° towards 088°) and SE (17° towards 146°). The thickness in the SE-dipping region is 8 m and thickness in the ENE-dipping region is 22 m. At the top, there is a conformable contact with Unit 6. The

upper part of Unit 6 comprises a fine-grained interval which is widely removed by an ~17 m deep erosion surface.

Units 10–18 are thicker (average 52 m), and comprise steeply-dipping (towards SE) foreset packages (Figure 9). Foresets are taller than those in the lower units (>100 m) (Figure 4). Bottomset outcrops at Locality VI (FA 4b; Figure 3) are positioned just above the projected plane from the top of Unit 12, and are therefore assigned to Unit 13. Outcrops at Localities VIII and IX (FA 4b; Figures 3 and 6) are positioned between the top of Unit 12 and the top of Unit 16. The Locality IX outcrop is E-dipping and is associated with Units 13–16. The Locality VIII outcrop is W-dipping (Kerinitis-derived) and stratigraphically higher, so deposited at the same time as Units 13-16, but after that at Locality IX. Outcrops at Localities X and XI (FA 4b; Figure 3) are positioned just below the projected plane for the top of Unit 16. The Locality X outcrop is E-dipping and assigned to Unit 16. The Locality XI outcrop is W-dipping and deposited at a similar time to the Locality X outcrop (Figure 3).

Unit set 3

Unit set 3 comprises Units 19-22 and is differentiated from Unit set 2 by the presence of shallower foreset dips, smaller preserved foreset heights (4–40 m), overall thinner units (average 16 m) and the interfingering of E and W-dipping beds (Figure 8). The dominant facies association is FA 3 (foresets). Unit 19 bedding (26° towards 127°; i.e. Selinous) shallows eastward, and is ~27 m thick. In the western part, it is eroded at the top. A ~7 m thick flat-lying fine-grained interval (3°
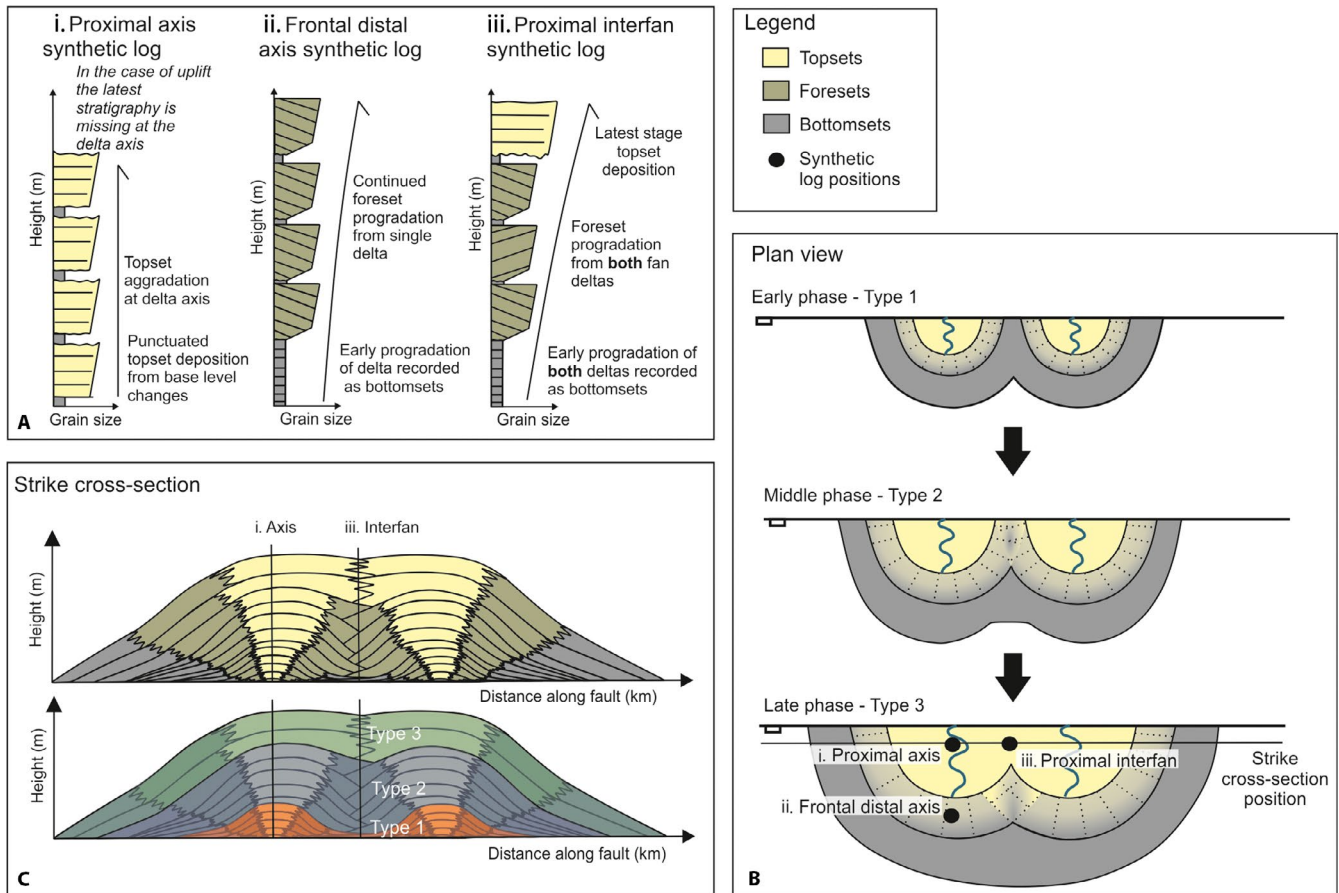
FIGURE 12 Typical evolution of an interfan through Types 1–3 with the progradation of two fan deltas. (A) Synthetic logs to show the differences in stratigraphic evolution between the delta axes and the interfan area. Synthetic logs are shown from the proximal axis (i), frontal distal axis (ii) and the interfan (iii). (B) Plan view evolution of the fan deltas, coalescing further as they grow and transitioning through interfan Types 1–3. (C) Strike cross-section through the proximal part of the deltas (position shown in B).

towards 154°) in the centre of Section 2 is interpreted to represent the correlative bottomsets (Figure 8). Unit 20 is also part of the Selinous fan delta, and its foresets downlap the erosion surface and the fine-grained interval at the centre of the outcrop. Unit 20 comprises thinner-bedded, smaller foresets than those in Unit set 2, although it is truncated at the top by an erosion surface (7° towards 154°). Within the unit, the bedding dip shallows eastward (from 16° towards 073°, to 7° towards 138°), but correlative bottomsets are not identified. Unit 21 is part of the Kerinitis fan delta and thins and shallows westward. In the area that it is thinnest, E-dipping, Selinous-derived beds (14–133°) interfinger and downlap W-dipping beds (10–233°). The E-dipping beds cannot be traced updip as they are eroded by the base Unit 22 surface. Unit 22 downlaps that surface and is distinct with thinly-bedded, small (4–5 m high) foresets dipping eastward (28° toward 148°—from Selinous). It is top truncated by a flat-lying erosion surface (Figure 8).

Unit set 4
Unit set 4 comprises Units 23 and 24, which are distinct from lower units as they have northward dip components (19° towards 015°), and in the west are flat-lying relative to

the underlying Unit set 2. Eastward, there is a sharp, angular lower contact with Unit 21, marked by downlap of Unit set 4 foresets. The top is not exposed, but the unit has a minimum thickness of 18 m. Limited exposures of Unit 24 are apparent in Section 3 (min. 20 m thick) (Figure 9), but outcrops are accessible at Locality I (FA 2c) (Figures 3 and 5).

4.3 | Interfan end-members

To augment the interpretation of the K–S interfan, a classification scheme is proposed for interfans using modern fan delta morphologies (Figure 2B). Interfans can be classified as one of three end-members according to their separation relative to fan delta topset and foreset radius, which determines the degree of interfingering of fan delta topset, foreset and bottomset deposits. The three types are presented in planform view and in strike cross-section in Figure 11, and with modern examples in Figure 2B. In Type 1, fan deltas are separated by a distance greater than the foreset radius and the interfan area is occupied by interfingering bottomset deposits. In Type 2, fan deltas are separated by a distance greater than the topset radius and less
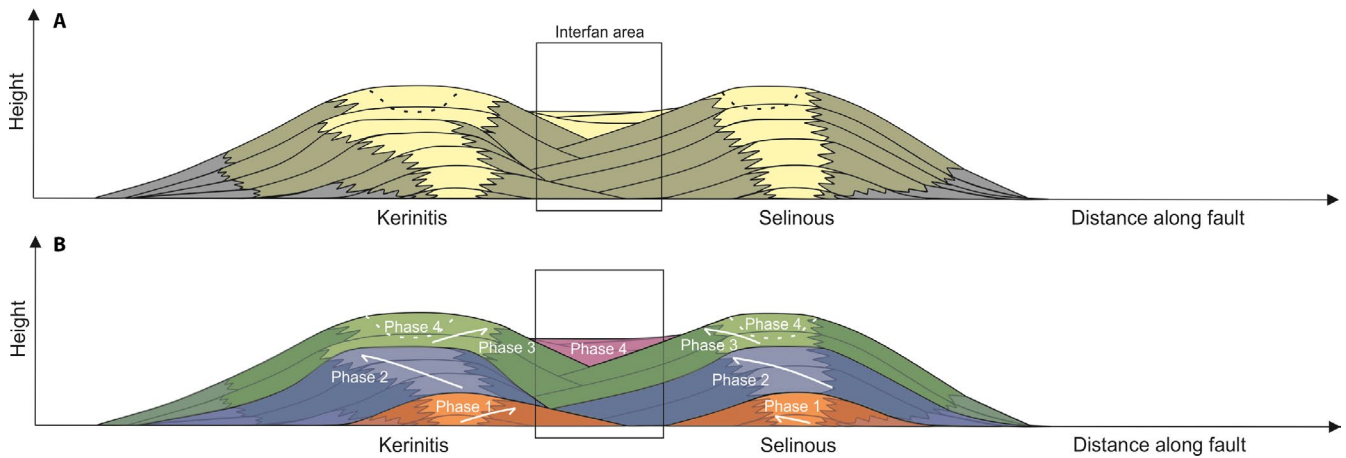
FIGURE 13 (A) Strike cross-section schematic diagram of the Early–Middle Pleistocene Kerinitis–Selinous interfan (grey box) large-scale architecture. (B) Diagram overlain with colours indicating Phases 1–4 of interfan evolution. Dashed lines indicate erosion during Phase 4. White arrows indicate progradation direction of each fan delta during each phase.

than the foreset radius, and both foresets and bottomsets interfinger in the interfan area. In Type 3, topsets, foresets and bottomsets interfinger as the fan delta systems are closely abutted at a distance less than the topset radius. The equivalent of a Type 3 interfan in an alluvial setting is a bajada (Blackwelder, 1931; Hooke, 1972; Bull, 1977; Miliaresis, 2001).

In each type, the interacting process regime and deposits will differ. When considering the evolution of an interfan, the geometry may evolve between these types and will depend largely on the allogenic forcing responsible for the building of the fan deltas and the basin evolution. Figure 12 shows a model for the evolution of an interfan area as two fan deltas prograde and coalesce. Three synthetic logs are presented to show the differences in the stratigraphic record through this process at different positions: the proximal axis, the distal axis and the interfan area. In this respect, each type can be considered as a single stage of evolution. This classification also represents the degree of coalescence in the dip direction. For example, an interfan could present Type 3 geometry in the proximal region and Types 2 and 1 with distance away from the sediment source (Figure 11C).

5 | INTERPRETATION OF THE K–S INTERFAN TEMPORAL EVOLUTION

The stratigraphic framework at Selinous and Kerinitis is presented as a fence diagram to illustrate an along-strike section across the interfan (Figure 9) and dip sections through the deltas axes (Figure 10; after Backert *et al.*, 2010; Gawthorpe *et al.*, 2017b; Barrett *et al.*, 2019). The interfan evolved through five distinct phases of progradation:

1. Initial progradation of the fan deltas into the interfan area, starting with Kerinitis.

2. Progradation of the Selinous fan delta into the interfan area and asymmetric eastward delta growth.
3. Aggradation and interfingering of the two systems, and shallowing of the interfan area.
4. Relative base-level fall, erosion and reworking of eroded sediments into the interfan area.
5. Continued uplift of the West Helike footwall and exposure of the Early–Middle Pleistocene deltas and growth of Late Pleistocene deltas in the West Helike hangingwall basin.

These phases are further described in the following sections and are presented in Figures 13 and 14.

5.1 | Phase 1 (Unit set 1)

Activity on the P–M Fault began ~1.8 Ma (Ford *et al.*, 2016) and hangingwall subsidence created space for sediments to accumulate. The Kerinitis and Selinous rivers cut through the uplifting footwall and fed sediment to the new hangingwall basin. The development of Gilbert-type fan deltas along the fault suggests that the fault line defined the coastline at this time. Displacement is greatest at fault centres (Walsh and Watterson, 1988; Dawers and Anders, 1995), resulting in the greatest accommodation at this position. The first unit apparent in the interfan area (Unit 1 within Unit set 1) is W-dipping and part of the Kerinitis fan delta, which sits closest to the fault centre. Unit 1 is not tied directly to the Kerinitis axial stratigraphy, but can be traced up-dip approximately to the middle units. This suggests that earlier progradation of Kerinitis did not extend as far as the interfan study area, and that the interfan is younger than early units deposited at the Kerinitis delta axis. It is unclear whether the progradation of the Kerinitis fan delta into the interfan area represents directional westward progradation, or overall expansion of the fan during this phase. There is no evidence that Selinous foresets prograded as far as

FIGURE 14 The Kerinitis–Selinous interfan evolution records: progradation of deltas into the interfan area (Phase 1), asymmetry of growth towards the east (Phase 2), stratal interfingering during net subsidence (Phase 3) and relative base-level fall, erosion and reworking during net uplift, as a result of a basinward fault set switch (Phases 4–5).
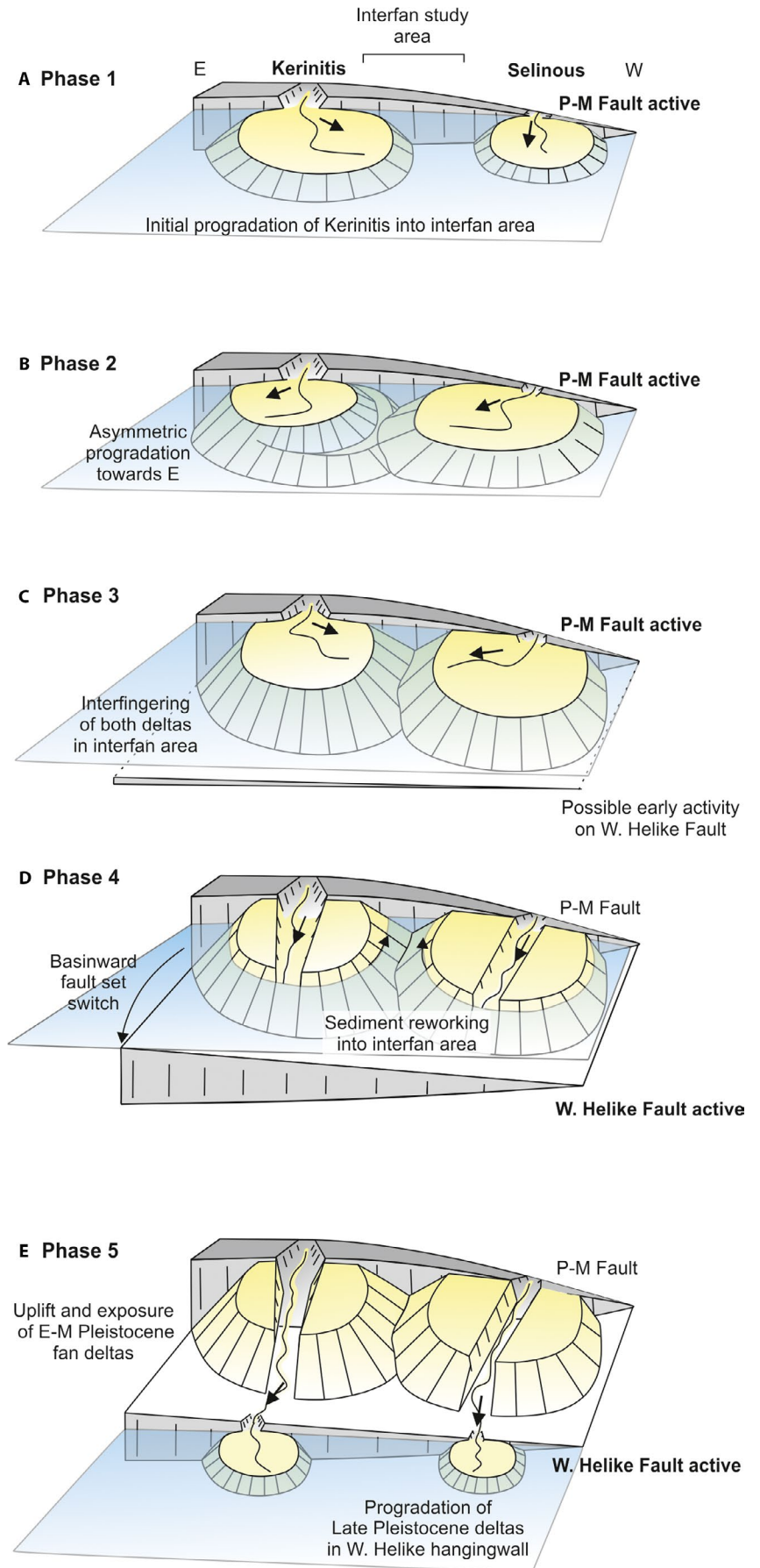
the interfan area during deposition of Unit set 1, as downlap at this location is only observed in later units. A plane projection of the top Unit 1 surface using the 3D outcrop model indicates that in the west, it sits below the earliest E-dipping units from Selinous. Hence, Kerinitis prograded into the interfan area before Selinous (Figures 13 and 14).

During Phase 1, the interfan can be classified as Interfan Type 1, separated by a distance greater than the radius of the foresets (Figure 11), as only Kerinitis foresets are evident in the interfan at this stage. It is not Type 2 because Selinous foresets are absent and thus the foresets of the two systems are not interfingering. Bottomset exposures in the interfan area linked to early Selinous progradation are not observed, but it is likely that fine-grained bottomset deposits were interfingering in the interfan area at this time.

5.2 | Phase 2 (Unit set 2)

During Phase 2, the Selinous fan delta began to prograde eastward into the interfan area, as indicated by E-dipping Unit set 2 (Units 2–18). Units 3–5 reveal topset-foreset breakpoint trajectories (Helland-Hansen and Hampson, 2009) at a distance of ~1 km from the fault (Section 4), suggesting the shoreline was proximal to the fault in the interfan area. The progradation–aggradational trajectory of Unit 3, suggests that sedimentation rate was high, and kept pace and exceeded the rate of accommodation creation. The progradational trajectory of Unit 4 suggests sedimentation rate exceeded the rate of accommodation creation, whereas the aggradational trajectory of Unit 5 suggests sedimentation rate kept pace with the rate of accommodation creation. The middle units at the Selinous delta axis present similar progradational–aggradational trajectories (Barrett *et al.*, 2019). Through the development of these three units the breakpoint remains in a similar position, suggesting overall aggradation (i.e. sedimentation kept pace with the rate of accommodation creation). In Unit 3, a full clinoform is preserved with a foreset height of 32 m, suggesting a ~30 m palaeo-water depth in the interfan area at this time. Foreset height increases to <200 m in Units 9–18. Foreset height increases as a result of the greater space available in the deeper water into which the foresets prograded. The fact that the foresets aggraded as well as prograded, suggests relative base-level rise outpaced sediment supply, most likely because of high subsidence rates of the P–M Fault hangingwall.

The E-dipping Unit 15 (Selinous-derived) downlaps onto the W-dipping Unit 1 (Kerinitis-derived; Unit set 1) (Figures 13 and 14). This is the first evidence of foresets interfingering between the two fan deltas. Units 16–19 continue to build up the flanks of these older Kerinitis foresets. They decreased in height as they built out into shallower water. At this stage, there is no evidence of Kerinitis building into the interfan area. Thus, Kerinitis was likely prograding to the north and east at this time. It is clear that there is an asymmetric architecture

in the interfan during Phase 2, with significant progradation from Selinous to the east, and inferred progradation from Kerinitis in the same direction. Presumably, therefore, both Selinous and Kerinitis exhibited asymmetric planform geometries, comparable to that of the modern Meganitis, Selinous, Kerinitis and Ladopotamos fan deltas (Figure 2).

During Phase 2, the interfan evolves from a Type 1 to Type 2 interfan (Figure 11) as foresets from both fan deltas are now apparent and interfingering in the interfan area. However, this interfingering occurred in two discrete phases, firstly from Kerinitis and then from Selinous (Figure 13), as opposed to continuous abutting (Figure 11).

5.3 | Phase 3 (Unit set 3)

Phase 3 is differentiated from Phase 2 by shallower dips, thinner units and continuous interfingering of E (Selinous) and W-dipping (Kerinitis) beds, which suggest a different depositional setting to Phase 2. During Phase 3, Selinous prograded eastward and Kerinitis prograded westward, into the interfan area (Unit set 3; Figures 13 and 14). Bedding dips within Unit 19 decrease laterally and have correlative bottomsets apparent in Section 2 (Figure 8). Unit 20 bed dips shallow upwards, and Units 20–22 are thinner than the preceding units (5–25 m thick), suggesting less available accommodation. Therefore, Selinous built into gradually shallower water as it encroached onto the Kerinitis margin. Sharp contacts formed as progradation from both systems caused foresets to downlap onto each other. Unit 22 comprises thinly-bedded, small (4–5 m high) foresets that are top truncated. Despite the truncation meaning that the true height of the foresets cannot be determined, water depth clearly shallowed significantly. Progradation occurred within the units, but generally the units aggraded, rather than prograded. This is likely to be a result of restricted lateral space as Selinous built up the flanks of Kerinitis, but with sufficient water depth for aggradation. The units thin towards the top of the section as they aggraded, which is likely to be due to decreasing activity on the P–M Fault causing reduced subsidence rates. Units 20 and 22 are truncated by major erosion surfaces. The top erosional contact of Unit 22 reveals a transition from small foresets to flat-lying beds that could be topsets. There is also a lack of fine-grained intervals towards the top of Unit set 3. This may be due to erosion, with the higher energy conditions limiting fine-grained sediment preservation. Alternatively, their formation was restricted by either: slowing subsidence rates reducing the rate of base-level rise such that climate-induced lake-level falls could overcome it, or new activity on the parallel, basinward West Helike Fault causing uplift of the footwall, and the associated overall relative base-level fall exceeding any climate-induced lake-level rises.

During Phase 3, the interfan continues to present the Type 2 interfan geometry, whereby foresets interfinger in the

interfan area. However, the foreset interfingering is expressed differently to that of Phase 2, with consistent abuttal, rather than discrete phases of progradation.

5.4 | Phase 4 (Unit set 4)

Unit set 4 (Units 23–24) developed during Phase 4. Unit set 4 is more flat lying than the steeply-dipping underlying units, has a northern component of dip and consists of metre-scale, well-sorted lenses of sand and conglomerate (FA 2b) that dip eastward and westward (Figures 5, 13 and 14). These are interpreted to represent subaqueous migrating bedforms that are made up of reworked material transported into the interfan area by wave-related longshore currents, for example, longshore bars (Orme, 1985; Ashley, 1990; Larson, and Kraus, 1992; Drønen and Deigaard, 2007). Some accommodation (shallow water) therefore existed in the interfan at this time. Activity on the P–M Fault ceased at ~0.7 Ma, at which time the West Helike Fault became active and dominant (Ford *et al.*, 2007). Uplift of the West Helike footwall caused the delta axes to become exposed above base-level (relative base-level fall). The uplift rate of the contiguous East Helike Fault is 1–1.5 mm/year (De Martini *et al.*, 2004), and the Kerinitis and Selinous rivers incised their own topsets. The modern geomorphology of the valleys shows that the main river direction and sediment pathway was, and continues to be, northwards. Unit set 4 deposits are interpreted to mark the erosion and reworking of topset material into the shallow interfan in response to basinward migration of strain and net basin uplift. The shallow water topsets from Selinous and Kerinitis were abutting at this time (Figure 13). The interfan therefore finally evolved to Type 3 during this phase.

5.5 | Phase 5

Phase 5 is not recorded in the interfan stratigraphy, but soil development and surficial erosion has occurred during and since Phase 5. Late Pleistocene fan deltas formed in the hangingwall of the West Helike Fault. By this time, the shoreline had therefore migrated to the West Helike Fault scarp. The Early–Middle Pleistocene fan deltas continued to be eroded by their feeder rivers (Figure 14).

In summary, the Kerinitis and Selinous interfan evolution can be divided into two parts according to the basin evolution (Figure 14). In the first part, growth of the P–M Fault caused net subsidence of the hangingwall basin and resulted in Phases 1–3 of interfan evolution: initial progradation of the fan deltas into the interfan area, starting with Kerinitis (Phase 1), asymmetric Selinous fan delta growth eastward (Phase 2), and interfingering of the two systems and shallowing of the interfan (Phase 3). In the second part, the P–M Fault ceased to be active and strain was accommodated on the West Helike Fault (basinward fault set switch), causing uplift of the West Helike Fault footwall and thus net uplift of the P–M Fault hangingwall basin through its transition from a marginal fault block to fault terrace. This resulted in relative base-level fall, erosion and reworking of sediments into the interfan area (Phase 4), and continued uplift until base-level fell below the West Helike fault scarp, which cut off the Early–Middle Pleistocene deltas and accommodated growth of Late Pleistocene fan deltas in the West Helike hangingwall basin (Phase 5).

6 | DISCUSSION

Based on observations of modern fan deltas and detailed analysis of the exhumed Early–Middle Pleistocene interfan between the Kerinitis and Selinous fan deltas, there emerges a more complete understanding of the stratal architecture resulting from along-strike interfingering of fan deltas during basin evolution. The following section discusses the classification scheme for interfans in terms of its applicability to other ancient systems, the mechanisms for the observed asymmetry in the ancient and modern systems, and the value of including interfan analysis in basin research.

6.1 | Style and classification of interfans

Proposed here is the first classification scheme for deltaic interfans based on modern fan delta geometries, which has been used to describe the evolution of the ancient system studied. Interfan styles are differentiated based on their separation relative to the radius of the delta topsets and foresets; this determines the interfingering of topsets, foresets and bottomsets in the interfan area (Figure 11). The interfan between the Kerinitis and Selinous fan deltas evolved from Type 1 (Phase 1) to Type 2 (Phases 2 and 3), and finally reached Type 3 (Phase 4). The interfan evolved through all three end-members (Figure 11). Although these types were characterised from, and represent end-members of modern systems (Figure 2B), they also represent an evolutionary continuum of an interfan, assuming a sufficient sediment supply and progradation that eventually occupies the distance between the fan deltas (Figure 12). It is also possible to use the classification scheme to subdivide an interfan in the dip direction (Figure 11C). In the exhumed system studied, it is the geometries proximal to the fault/sediment source that are considered for the classification (strike line presented in Figure 11). However, in a case with topsets adjoined in the proximal area (Type 3), the interfan will also exhibit Type 2 and Type 1 in a proximal to distal trend (Figure 11C).

The scheme is presented with adjacent fan deltas in the hangingwall of a fault, but it is worth noting that the scheme also applies to adjacent systems in the footwall, and also fans that are obliquely prograding. For example, one fan

prograding down a relay ramp may coalesce with one in the immediate hangingwall and the classification scheme is still applicable (Figure 2B).

6.2 | Asymmetry of fan deltas

In previously published models of fan deltas in rift settings (Gawthorpe and Leeder, 2000), and in the interfan models presented here (Figure 11), a symmetrical planform geometry and architecture of fan deltas is assumed. This follows the originally described Gilbert-type fan delta descriptions from the tectonically quiescent Lake Bonneville (e.g. American Fork delta; Gilbert, 1890; Milligan and McDonald, 2016) that were principally controlled by lacustrine base-level change in a glacial climate and which exhibit a symmetrical delta architecture (Gilbert, 1890; Lemons *et al.*, 1996; Godsey *et al.*, 2005). However, it is clear that during Phase 2 the Selinous fan delta, and most likely the Kerinitis fan delta, were asymmetric, and skewed eastward (Figures 13 and 14). Many of the modern fan deltas along the southern shore of the Gulf of Corinth also have an asymmetric delta plain geometry, representing a snap-shot of their tectono-stratigraphic evolution (e.g. the Meganitis, Selinous, Kerinitis and Akrata fan deltas; Figure 2A,2). The definition of the interfan is proposed here as 'the area between two lines that project from the apices of two fan deltas to their intersection at the most distal point of bottomset interfingering' is applicable to asymmetric fans, but the limit of distal interfingering is more challenging to pinpoint in these cases.

There are two potential mechanisms for this asymmetry: (a) preferential reworking of sediments from the dominant wind and wave direction and/or, (b) principal sediment supply towards structural lows. In the modern Gulf of Corinth, a westerly wind and wave direction prevails, conditions that are expected to have been similar in the Early–Middle Pleistocene. The carrying energy of the longshore current would have been dependent on the weather conditions, with local storms producing currents with a higher energy that allow greater loads to be transported along-shore (Bagnold, 1966). A number of formulas have been derived to predict longshore sediment transport in swell and storm conditions (Bijker, 1967; Engelund and Hansen, 1967; Ackers and White, 1973; Van de Graaff and Van Overeem, 1979; Bailard and Inman, 1981; Van Rijn, 1984; Watanabe *et al.*, 1991); and these are compared in Bayram *et al.* (2001). As a result, sediments above wave base have been pervasively reworked eastward. This is a likely mechanism for the skewing of planform topset geometry in the modern fan deltas (Figure 2A,2) and may have driven migration of the barforms present in Unit 24 of the K–S interfan (Figure 5). In cases where shallow water foresets have prograded over a previously flooded delta topset there is also the potential for longshore current reworking. For example, the foresets of the modern Selinous delta that overlie the submerged Late Pleistocene Selinous fan delta (Figure 2B).

For the overall fan delta architecture to be asymmetrical, there must be a driver to deflect the rivers. Differential subsidence along the border faults results in structural gradients, where the lowest point typically lies at the fault centre (Walsh and Watterson, 1988; Dawers and Anders, 1995). Over time, the rivers and resultant fan deltas preferentially follow the structural contours. A structural influence on river course has been documented for the modern Selinous and Kerinitis rivers. The modern Kerinitis River has migrated towards the north–west since AD 450-1400 (Schmidt, 1879; Soter and Katsonopoulou, 1998; McNeill and Collier, 2004) as a result of differential displacement in the relay zone between the East and West Heliki Faults (Figure 2). The modern Selinous River has gradually migrated towards the south-east in response to growth of the Aigion Fault (Soter and Katsonopoulou, 1998; McNeill and Collier, 2004; Figure 2). Asymmetry of fan delta architecture should be expected in tectonically-active settings subjected to differential subsidence. Interfans in these settings are therefore likely to exhibit a dominant influence from one fan delta, as can be seen in the K–S interfan, where the Selinous fan delta dominates during Phase 2. The highest rates of hangingwall subsidence are interpreted during Phase 2, which coincides with the most pronounced asymmetry. Ultimately, the degree of asymmetry through time is controlled by the interplay of external controls. In rift basins, this can be complicated by fault segment linkage that influences along-strike subsidence patterns. If the fan deltas prograde towards the area with more subsidence, which may change its position through time, the rivers will respond to change the dominant system in the interfan area.

In summary, the observed asymmetry in the ancient succession is architectural, with large foresets from the Selinous fan delta dominating the interfan succession (Figures 9 and 13), and thus reflecting a response to the structural gradient towards the fault centre. The asymmetry observed in the planform geometry of the modern fan deltas (Figure 2), and in the higher units of the interfan (Figure 8), is more likely to be a result of the prevailing wind and wave direction.

6.3 | Interfans as stratigraphic archives

Interactions of tectonics, base level and sediment supply are spatially and temporally complex. Interfan stratigraphy can record the complexity of the temporal evolution in rift settings, and the transition from net subsidence to net uplift, which is not recorded stratigraphically at the fan delta axes. Here, this regime shift was the result of a 6 km northward (basinward) transfer of fault activity from the P–M Fault to the West Helike Fault, and is recorded by (a) an overall shallowing upwards facies trend from Unit set 2–4, (b) reduced foreset heights, (c) a vertical stacking pattern suggesting a restriction of lateral space, (d) a greater number of units in the interfan than at the delta axes, and (e) subsequent erosion and

progradation of younger fan deltas in the hangingwall of the West Helike Fault. During basin uplift, due to its deeper water position, the K–S interfan retained accommodation for longer than the delta axes, which became exposed first. Although, the axial parts of fan deltas record the earliest phases of delta evolution, prior to progradation into the interfan area, the K–S interfan provides a more complete stratigraphic record of the final stages of delta evolution (Figures 13 and 14). In Figure 12, synthetic logs are presented to show the differences in the stratigraphic record at three positions through the progradation of two fan deltas: the proximal axis, the frontal distal axis and the interfan area. The proximal axis records the aggradation of topset units from the earliest growth phase, but in the case of uplift, is missing the latest stage of evolution. At the frontal distal axis, the earliest progradation of a single fan delta is recorded with bottomset deposits, and becomes overlain by foresets from that fan delta. As it is in a deeper water position, the frontal distal axis continues to preserve stratigraphy during the latest stage, but only from one fan delta. The proximal interfan records the early progradation of both fan deltas as interfingering bottomset deposits. The middle phase is represented by the progradation of foresets from both fan deltas and the latest stage is occupied by topset deposition. Thus, the interfan area not only provides a more complete record through uplift, but also records the history of both fan deltas, their architectural interactions through time, and potentially reveals their asymmetry more readily than in axial dip sections. Both the axial and interfan areas are complementary and together yield the most complete record of basin evolution (Figure 12), which has high utility. For example, if more complete biostratigraphic and palaeomagnetic records were available from fine-grained intervals and with more accurate correlation of stable, cosmogenic and radiogenic isotope curves to the fan delta succession, greater confidence in dating and tying of the eustatic sea-level curve to the stratigraphy could be achieved (Emiliani, 1955; Imbrie *et al.*, 1984; Lisiecki and Raymo, 2005). Interfan areas could therefore represent valuable but underutilised stratigraphic archives, which merit further investigation.

7 | CONCLUSIONS

This is the first detailed study of syn-rift stratigraphic architectures in the interfan area of coeval fan deltas. Field data and UAV photogrammetry-based 3D outcrop models are used to extract qualitative and quantitative data from the Early–Middle K–S interfan. Modern planform geometries of interfan areas allow the classification of interfans into three end-members based on their separation according to delta topset and foreset radius, which can be applied to ancient systems. The Early–Middle Pleistocene K–S interfan evolved from Type 1 to Type 3 through five evolutionary phases from net subsidence to net uplift, due to a northward migration of fault activity from the P–M Fault to the West Helike Fault. The interfan architectures record: early progradation of the Kerinitis delta into the interfan area (Phase 1), subsequent progradation of the Selinous delta into the interfan area and asymmetry of growth of both fan deltas eastward (Phase 2), stratal interfingering of foresets from both fan deltas during net subsidence (Phase 3), and relative base-level fall, erosion and reworking during net uplift, as a result of a basinward fault set switch (Phases 4 and 5). Planform asymmetry in the modern fan deltas is interpreted to be a result of wind and wave directional reworking. Architectural asymmetry is interpreted to be due to preferential river avulsion towards structural lows driven by subsidence patterns along active faults. Thus, architectural asymmetry may be a common feature in rift basins, and as such interfans in these settings are likely to preserve evidence of a dominant depositional system. Interfan areas provide a condensed, and potentially more complete, stratigraphic record than the axial areas of the fan deltas through high preservation potential and longer submergence during the early stages of basin uplift, and therefore allow further insight into basin evolution. Interfan areas are underrepresented in terms of their importance in the literature, yet could be exploited as important stratigraphic archives that complement fan delta axial records.

CONFLICT OF INTEREST

The authors confirm that they have no affiliations with or involvement in any organization or entity with any financial or non-financial interest in the subject matter or materials discussed in this manuscript.

DATA AVAILABILITY STATEMENT

The data that support the findings of this study are available from the corresponding author upon reasonable request.

ORCID

Bonita J. Barrett ID https://orcid.org/0000-0002-3274-822X

Rob L. Gawthorpe ID https://orcid.org/0000-0002-4352-6366

Richard E. Ll. Collier ID https://orcid.org/0000-0002-8001-0510

David M. Hodgson ID https://orcid.org/0000-0003-3711-635X

Timothy M. Cullen ID https://orcid.org/0000-0002-2497-2213

REFERENCES

Ackers, P. and White, W.R. (1973) Sediment transport: new approach and analysis. *Journals of Hydraulics Division*, *99*, 2041–2060.

Ashley, G.M. (1990) Classification of large-scale subaqueous bedforms: a new look at an old problem. *Journal of Sedimentary Research*, *60*, 160–172.

Assine, M.L., Renato Merino, E., Do Nascimento Pupin F., De Azevedo Macedo, H. and Guerreiro Martinho Dos Santos, M. (2015) The Quaternary alluvial systems tract of the Pantanal Basin, Brazil. *Brazilian Journal of Geology*, *45*(3), 475–489.

Avallone, A., Briole, P., Agatza-Balodimou, A.M., Billiris, H., Charade, O., Mitsakaki, C. *et al.* (2004) Analysis of eleven years of deformation measured by GPS in the Corinth Rift Laboratory area. *Comptes Rendus Geoscience*, *336*, 301–311.

Backert, N., Ford, M. and Malartre, F. (2010) Architecture and sedimentology of the Kerinitis Gilbert-type fan delta, Corinth Rift, Greece. *Sedimentology*, *57*, 543–586.

Bailard, J.A. and Inman, D.L. (1981) An energetics bedload model for plane sloping beach: local transport. *Journal of Geophysical Research*, *86*, 2035–2043.

Barrett, B., Hodgson, D.M., Collier, R.E.Ll, Collier, R.E.Ll and Dorrell, R.M. (2018) Novel 3D sequence stratigraphic numerical model for syn-rift basins: analysing architectural responses to eustasy, sedimentation and tectonics. *Marine and Petroleum Geology*, *92*, 270–284. Available at: doi:https://doi.org/10.1016/j.marpetgeo.2017.10.026.

Barrett, B., Collier, R.E.L.L., Hodgson, D.M., Gawthorpe, R.L., Dorrell, R.M. and Cullen, T.M. (2019) Quantifying faulting and base level controls on syn-rift sedimentation using stratigraphic architectures of coeval fan deltas: constraining Early-Middle Pleistocene base-level amplitude change in Lake Corinth. *Basin Research*. Available at: doi:https://doi.org/10.1111/bre.12356.

Bagnold, R.A. (1966) An approach to the sediment transport problem from general physics. Geological Survey Professional Paper. Washington: United States Government Printing Office, 37pp.

Bayram, A., Larson, M., Miller, H.C. and Kraus, N.C. (2001) Cross-shore distribution of longshore sediment transport: comparison between predictive formulas and field measurements. *Coastal Engineering*, *44*, 79–99.

Bell, D., Stevenson, C.J., Kane, I.A., Hodgson, D.M. and Poyatos-Moré, M. (2018) Topographic controls on the development of contemporaneous but contrasting basin-floor depositional architectures. *Journal of Sedimentary Research*, *88*, 1166–1189.

Bhiry, N. and Occhietti, S. (2004) Fluvial sedimentation in a semi-arid region: the fan and interfan system of the Middle Souss Valley, Morocco. *Proceedings of the Geologists' Association*, *115*, 313–324.

Bijker, E.W. (1967) Some considerations about scales for coastal models with movable bed. Delft Hydraulics Laboratory, Publication

50, Delft, the Netherlands. *Journal of the Waterways, Harbors and Coastal Engineering Division*, *97*, 687.

Blackwelder, E. (1931) Desert plains. *Journal of Geology*, *39*, 133–140.

Briole, P., Rigo, A., Lyon-Caen, H., Ruegg, J.C., Papazissi, K., Mitsakaki, C. *et al.* (2000) Active deformation of the Corinth rift, Greece: Results from repeated Global Positioning System surveys between 1990 and 1995. *Journal of Geophysical Research-Solid Earth*, *105*, 25605–25625.

Bull, W. (1977) The alluvial fan environment. *Progress in Physical Geography*, *1*, 222–270.

Capraro, L., Asioli, A., Backman, J., Bertoldi, R., Channell, J.E.T., Massari, F. *et al.* (2005) Climatic patterns revealed by pollen and oxygen isotope records across the Matuyama-Brunhes boundary in the central Mediterranean (southern Italy). *Geological Society, London, Special Publications*, *247*, 159–182.

Clarke, P.J., Davies, R.R., England, P.C., Parsons, B.E., Billiris, H., Paradissis, D. *et al.* (1997) Geodetic estimate of seismic hazard in the Gulf of Korinthos. *Geophysical Research Letters*, *24*, 1303–1306.

Collier, R.E.Ll. (1990) Eustatic and tectonic controls upon Quaternary coastal sedimentation in the Corinth Basin, Greece. *Journal of the Geological Society*, *147*, 301–314.

Collier, R.E.Ll. and Dart, C.J. (1991) Neogene to Quaternary rifting, sedimentation and uplift in the Corinth Basin, Greece. *Journal of the Geological Society, London*, *148*, 1049–1065.

Collier, R.E.Ll. and Thompson, J. (1991) Transverse and linear dunes in an Upper Pleistocene marine sequence, Corinth Basin, Greece. *Sedimentology*, *38*, 1021–1040.

Collier, R.E.Ll., Leeder, M.R., Trout, M., Ferentinos, G., Lyberis, E. and Papatheodorou, G. (2000) High sediment yields and cool, wet winters: test of last glacial paleoclimates in the northern Mediterranean. *Geology*, *28*, 999–1002.

Cotterill, C.J. (2002) A high resolution Holocene fault activity history of the Aigion shelf, Gulf of Corinth, Greece. PhD Thesis, School of Ocean and Earth Sciences, University of Southampton.

Covault, J.A. and Graham, S.A. (2010) Submarine fans at all sea-level stands: tectonomorphologic and climatic controls on terrigenous sediment delivery to the deep sea. *Geology*, *38*, 939–942.

Dart, C.J., Collier, R.E.L., Gawthorpe, R.L., Keller, J.V.A. and Nichols, G. (1994) Sequence stratigraphy of (?)Pliocene-quaternary synrift, gilbert-type fan deltas, Northern Peloponnesos, Greece. *Marine and Petroleum Geology*, *11*, 545–560.

Dawers, N.H. and Anders, M.H. (1995) Displacement-length scaling and fault linkage. *Journal of Structural Geology*, *17*, 607–614.

De Martini, P., Pantosti, D., Palyvos, N., Lemeille, F., McNeill, L. and Collier, R.E.Ll. (2004) Slip rates of the Aigion and Eliki faults from uplifted marine terraces, Corinth Gulf, Greece. *Comptes Rendus Geoscience*, *336*, 325–334.

Degnan, P.J. and Robertson, A.H.F. (1998) Mesozoic-early Tertiary passive margin of the Pindos ocean (NW Peloponnese, Greece). *Sedimentary Geology*, *117*, 33–70.

Dodenov, A.E. (2005) The stratigraphic transition and suggested boundary between the Early and Middle Pleistocene in the loess record of northern Eurasia. *Geological Society, London, Special Publications*, *247*, 209–219.

Drønen, N. and Deigaard, R. (2007) Quasi-three-dimensional modelling of the morphology of longshore bars. *Coastal Engineering*, *54*, 197–221.

Emiliani, C. (1955) Pleistocene temperatures. *Journal of Geology*, *63*, 538–578.

Emiliani, C. (1978) The cause of the ice ages. *Earth & Planetary Science Letters*, *37*, 349–352.

Engelund, F. and Hansen, E. (1967) *A Monograph On Sediment Transport in Alluvial Streams*. Copenhagen, Denmark: Teknisk Forlag.

Floyd, M.A., Billiris, H., Paradissis, D., Veis, G., Avallone, A., Briole, P. *et al.* (2010) A new velocity field for Greece: implications for the kinematics and dynamics of the Aegean. *Journal of Geophysical Research*, 115, B10403.

Ford, M., Williams, E.A., Malartre, F. and Popescu, S.M. (2007) Stratigraphic architecture, sedimentology and structure of the Vouraikos Gilbert-type fan delta, Gulf of Corinth, Greece. In: Nichols, G., Williams, E. and Paola, C. (Eds.) *Sedimentary Processes, Environments and Basins. A Tribute to Peter Friend. International Association of Sedimentology Special Publications*, 38, 49–90.

Ford, M., Rohais, S., Williams, E.A., Bourlange, S., Jousselin, D., Backert, N. *et al*. (2013) Tectonosedimentary evolution of the western Corinth rift (Central Greece). *Basin Research*, 25, 3–25.

Ford, M., Hemelsdael, R., Mancini, M. and Palyvos, N. (2016) Rift migration and lateral propagation: evolution of normal faults and sediment-routing systems of the western Corinth rift (Greece). In: Childs, C., Holdsworth, R.E., Jackson, C.A.-L., Manzocchi, T., Walsh, J.J. and Yielding, G. (Eds.) *The Geometry of Normal Faults. Geological Society, London, Special Publications*, 439, 131–168.

Gawthorpe, R.L. and Leeder, M.R. (2000) Tectono-sedimentary evolution of active extensional basins. *Basin Research*, 12, 195–218.

Gawthorpe, R.L., Fraser, A. and Collier, R.E.Ll. (1994) Sequence stratigraphy in active extensional basins: implications for the interpretation of ancient basin fills. *Marine and Petroleum Geology*, 11, 642–658.

Gawthorpe, R.L., Sharp, I., Underhill, J.R. and Gupta, S. (1997) Linked sequence stratigraphic and structural evolution of propagating normal faults. *Geology*, 25, 795–798.

Gawthorpe, R.L., Leeder, M.R., Kranis, H., Skourtsos, E., Andrews, J.E., Henstra, G.A. *et al.* (2017a) Tectono-sedimentary evolution of the Plio-Pleistocene Corinth rift, Greece. *Basin Research*, 30, 1–32. Available at: doi:https://doi.org/10.1111/bre.12260.

Gawthorpe, R.L., Andrews, J.E., Collier, R.E.L., Ford, M., Henstra, G.A., Kranis, H., *et al.* (2017b) Building up or out? Disparate sequence architectures along an active rift margin – Corinth rift, Greece. *Geology*, 45, 111–114.

Ghisetti, F. and Vezzani, L. (2004) Plio-Pleistocene sedimentation and fault segmentation in the Gulf of Corinth (Greece) controlled by inherited structural fabric. *Comptes Rendus Geosciences*, 336, 243–249.

Gilbert, G.K. (1890) Lake Bonneville. *U.S. Geological Survey Monograph*, 1, 438.

Gobo, K., Ghinassi, M. and Nemec, W. (2014) Reciprocal changes in foreset to bottomset facies in a gilbert-type delta: Response to short-term changes in base level. *Journal of Sedimentary Research*, 84, 1079–1095.

Gobo, K., Ghinassi, M. and Nemec, W. (2015) Gilbert-type deltas recording short-term base-level changes: Delta-brink morphodynamics and related foreset facies. *Sedimentology*, 62, 1923–1949.

Godsey, H.S., Currey, D.R. and Chan, M.A. (2005) New evidence for an extended occupation of the Provo shoreline and implications for regional climate change, Pleistocene Lake Bonneville, Utah, USA. *Quaternary Research*, 63, 212–223.

Goldsworthy, M. and Jackson, J. (2001) Migration of activity within normal fault systems: examples from the Quaternary of mainland Greece. *Journal of Structural Geology*, 23, 489–506.

Hardy, S. and Gawthorpe, R.L. (1998) Effects of variations in fault slip rate on sequence stratigraphy in fan deltas: insights from numerical modeling. *Geology*, 26, 911–914.

Head, M.J. and Gibbard, E.L. (2005) Early-Middle Pleistocene transitions: an overview and recommendation for defining the boundary. In: Head, M.J. and Gibbard, P.L. (Eds.), *Early-Middle Pleistocene Transitions: The Land-Ocean Evidence. Geological Society, London, Special Publications*, 247, 1–18.

Helland-Hansen, W. and Hampson, G.J. (2009) Trajectory analysis: concepts and applications. *Basin Research*, 21, 454–483.

Higgs, R. (1990) Sedimentology and tectonic implications of Cretaceous fan-delta conglomerates, Queen Charlotte Islands, Canada. *Sedimentology*, 37, 83–103.

Hodgson, D.M., Kane, I.A., Flint, S.S., Brunt, R.L. and Ortiz-Karpf, A. (2016) Time-transgressive confinement on the slope and the progradation of basin-floor fans: implications for the sequence stratigraphy of deep-water deposits. *Journal of Sedimentary Research*, 86, 73–86.

Hook, J., Abhvani, A., Gluyas, J.G. and Lawlor, M. (2003). The Birch Field, Block 16/12a, UK North Sea. In: Gluyas, J.G. and Hichens, H.M. (Eds.) *United Kingdom Oil and Gas Fields', Commemorative Millennium Volume. Geological Society, London, Memoir*, 20, 167–181.

Hooke, R. (1972) Geomorphic evidence for late-Wisconsin and Holocene tectonic deformation, Death Valley, California. *Geological Society of America Bulletin*, 83, 2073–2098.

Imbrie, J., Hays, J.D., Martinson, D.G., McIntyre, A., Mix, A.C., Morley, J.J. *et al.* (1984) The orbital theory of Pleistocene climate: Support from a revised chronology of the marine delta ^{18}O record. In: Berger, A. (Ed.) *Milankovitch and Climate*. Dordrecht, The Netherlands: Plenum Reidel, pp. 269–305.

Kneller, B., Edwards, D., McCaffery, W. and Moore, R. (1991) Oblique reflection of turbidity currents. *Geology*, 19, 250–252.

Larson, M. and Kraus, N.C. (1992) Dynamics of longshore bars. In: Edge, B.L. (Ed.), *Proceedings of 23rd Conference on Coastal Engineering*, Venice, Italy, 23, 2219–2232.

Leeder, M.R. and Gawthorpe, R.L. (1987) Sedimentary models for extensional tilt block/half-graben basins. In: Coward, M.P., Dewey, J.F. and Hancock, P.L. (Eds.), *Continental Extensional Tectonics. Geological Society, London, Special Publications*, 28, 139–152.

Leeder, M.R., Collier, R.E.Ll, Abdul Aziz, L.H., Trout, M., Ferentinos, G. and Papatheodorou, G. (2002) Tectono-sedimentary processes along an active marine/lacustrine half-graben margin: Alkyonides Gulf, E. Gulf of Corinth, Greece. *Basin Research*, 14, 25–41.

Leeder, M.R., Mack, G.H., Brasier, A.T., Parrish, R.R., Mintosh, W.C., Andrews, J.E. *et al.* (2008) Late-Pliocene timing of Corinth (Greece) rift-margin fault migration. *Earth and Planetary Science Letters*, 274, 132–141.

Lemons, D.R., Milligan, M.R. and Chan, M.A. (1996) Paleoclimatic implications of late Pleistocene sediment yield rates for the Bonneville Basin, northern Utah. *Palaeogeography, Palaeoclimatology, Palaeoecology*, 123, 147–159.

Leppard, C.W. and Gawthorpe, R.L. (2006) Sedimentology of rift climax deep water systems; Lower Rudeis Formation, Hammam Faraun Fault Block, Suez Rift, Egypt. *Sedimentary Geology*, 191, 67–87.

Lisiecki, L.E. and Raymo, M.E. (2005) A Pliocene-Pleistocene stack of 57 globally distributed benthic delta 18O records. *Paleoceanography*, 20, PA1003. Available at: doi:https://doi.org/10.1029/2004PA001071.

Lisiecki, L.E. and Raymo, M.E. (2007) Plio-Pleistocene climate evolution: trends and transitions in glacial cycle dynamics. *Quaternary Science Reviews*, 26, 56–69.

Lomas, S.A. and Joseph, P. (2004) Confined turbidite systems. In: Lomas, S.A. and Joseph, P. (Eds.) *Confined Turbidite Systems. Geological Society, London, Special Publications*, 222, 1–7.

McNeill, L.C. and Collier, R. (2004) Uplift and slip rates of the eastern Eliki fault segment, Gulf of Corinth, Greece, inferred from Holocene and Pleistocene terraces. *Journal of the Geological Society*, 161, 81–92.

McNeill, L.C., Collier, R.E.LL., De Martini, P.M., Pantosti, D. and D'Addezio, G. (2005) Recent history of the Eastern Eliki Fault, Gulf of Corinth: geomorphology, palaeoseismology and impact on palaeoenvironments. *Geophysical Journal International*, 16, 154–166.

Miliaresis, G.Ch. (2001) Extraction of bajadas from digital elevation models and satellite imagery. *Computers & Geosciences*, 27, 1157–1167.

Milligan, M. and McDonald, G. (2016) Shorelines and vertebrate fauna of Pleistocene Lake Bonneville, Utah, Idaho and Nevada. Geology of the Intermountain West, 4. A Field Guide Prepared for Society of Vertebrate Paleontology Annual Meeting, October 26–29, 2016 Grand America Hotel Salt Lake City, Utah, USA.

Moretti, I., Lykousis, V., Sakellariou, D., Reynaud, J.Y., Benziane, B. and Prinzhoffer, A. (2004) Sedimentation and subsidence rate in the Gulf of Corinth: what we learn from the Marion Dufresne's long-piston coring. *Comptes Rendus Geoscience*, 336, 291–299.

Nemec, W. (1990) Aspects of sediment movement on steep delta slopes. In: Collela, A. and Prior, D.B. (Eds.) *Coarse-Grained Deltas. Special Publications of International Association of Sedimentology*, 10, 29–73.

Nixon, C.W., McNeill, L.C., Bull, J.M., Bell, R.E., Gawthorpe, R.L., Henstock, T.J. *et al.* (2016) Rapid spatiotemporal variations in rift structure during development of the Corinth Rift, central Greece. *Tectonics*, 35, 1225–1248.

Ori, G.G., Roveri, M. and Nichols, G. (1991) Architectural patterns in large-scale Gilbert-type delta complexes, Pleistocene, Gulf of Corinth, Greece. In: Miall, A.D. and Tyler, N. (Eds.) *The Three Dimensional Facies Architecture if Terrigenous Clastic Sediments and its Implications for Hydrocarbon Discovery and Recovery. SEPM, Concept in Sedimentology and Paleontology*, pp. 207–216.

Orme, A.R. (1985) The behaviour and migration of longshore bars. *Physical Geography*, 6, 142–164.

Orton, G.J. and Reading, H.G. (1993) Variability of deltaic processes in terms of sediment supply, with particular emphasis on grain size. *Sedimentology*, 40, 475–512.

Postma, G. (1984) Slumps and their deposits in fan delta front and slope. *Geology*, 12, 27–30.

Potter, P.E. and Pettijohn, F.J. (1977) *Paleocurrents and Basin Analysis*, 2nd edn. New York, NY: Springer-Verlag, 425 p.

Poulimenos, G., Zelilidis, A., Kontopoulos, N. and Doutsos, T. (1993) Geometry of trapezoidal fan deltas and their relationship to extensional faulting along the south-western active margins of the Corinth rift, Greece. *Basins Research*, 5, 179–192.

van Rijn, L.C. (1984) Sediment transport: part I: bed load transport; Part II: suspended load transport; Part III: bed forms and alluvial roughness. *Journal of Hydraulic Division*, 110, 1431–1754.

Rohais, S. and Moretti, I. (2017) Structural and stratigraphic architecture of the Corinth rift (Greece): an integrated onshore to offshore basin-scale synthesis. In: Roure, F., Amin, A.A, Khomsi, S. and Al Garni, M.A.M. (Eds.) *Lithosphere Dynamics and Sedimentary Basins of the Arabian Plate and Surrounding Areas. Frontiers in Earth Sciences*, 89–120. Available at: doi:https://doi.org/10.1007/978-3-319-44726-1_5.

Rohais, S., Eschard, R., Ford, M., Guillocheau, F. and Moretti, I. (2007a) Stratigraphic architecture of the Plio-Pleistocene infill of the Corinth Rift: implications for its structural evolution. *Tectonophysics*, 440(1), 5–28.

Rohais, S., Joannin, S., Colin, J.P., Suc, J.P., Guillocheau, F. and Eschard, R. (2007b) Age and environmental evolution of the syn-rift fill of the southern coast of the gulf of Corinth (Akrata-Derveni region, Greece). *Bulletin de la Societe Geologique de France*, 178, 231–243.

Rohais, S., Eschard, R. and Guillocheau, F. (2008) Depositional model and stratigraphic architecture of rift climax Gilbert-type fan deltas (Gulf of Corinth, Greece). *Sedimentary Geology*, 210, 132–145. Available at: doi:https://doi.org/10.1016/j.sedgeo.2008.08.001.

Schmidt, J. (1879) *Studien uber Erdbeben*. Leipzig: Alwin Georgi, pp. 68–83.

Sohn, Y.K. (2000) Coarse-grained debris-flow deposits in the Miocene fan deltas, SE Korea: a scaling analysis. *Sedimentary Geology*, 130, 45–64.

Sohn, Y.K., Kim, S.B., Hwang, I.G., Bahk, J.J., Choe, M.Y. and Chough, S.K. (1997) Characteristics and depositional processes of large-scale gravelly Gilbert-type foresets in the Miocene Doumsan fan delta, Pohang Basin, SE Korea. *Journal of Sedimentary Research*, 67, 130–141.

Soter, S. and Katsonopoulou, D. (1998) The search for ancient Helike, 1988–1995: geological, sonar and bore hole studies. In: Katsonopoulou, D., Soter, S. and Scilardi, D. (Eds.) *Ancient Helike and Aigalieia*. Aigion, Greece: The Helike Society, pp. 67–116.

Stevenson, C.J., Jackson, C.A.-L., Hodgson, D.M., Hubbard, S.M. and Eggenhuisen, J.T. (2015) Deep-water sediment bypass. *Journal of Sedimentary Research*, 85, 1058–1081.

Suc, J.-P. and Popescu, S.-M. (2005) Pollen records and climatic cycles in the North Mediterranean region since 2.7 Ma. In: Head, M.J. and Gibbard, P.L. (Eds.) *Early-Middle Pleistocene Transitions: The Land-Ocean Evidence. Geological Society, London, Special Publications*, 247, 147–158.

Turner, C.C. and Connell, E.R. (2018) Mid to Late Jurassic graben margin development and evolution of shallow marine to submarine fan systems in the Brae area of the South Viking Graben, U.K. North Sea. In: Turner, C.C. and Cronin, B.T. (Eds.) *Rift-related Coarse-Grained Submarine Fan Reservoirs: The Brae Play, South Viking Graben, North Sea. AAPG Memoir*, 115, 163–212.

Van De Graaff J. and Van Overeem, J. (1979) Evaluation of sediment transport formulae in coastal engineering practice. *Coastal Engineering*, 3, 1–32.

Von Freyberg, B. (1973) Geologie des Isthmus von Korinth. Erlanger Geologische Abhandlungen, 95. Junge und Sohn, Universitats-Buchdruckerei, Erlangen.

Walsh, J.J. and Watterson, J. (1988) Analysis of the relationship between displacements and dimensions of faults. *Journal of Structural Geology*, 10, 239–247.

Watanabe, A., Shimizu, T. and Kondo, K. (1991) Field application of a numerical model for beach topography change. *Proceedings of Coastal Sediments*, 91, 1814–1829.

Young, M.J., Gawthorpe, R.L. and Sharp, I.R. (2002) Architecture and evolution of the syn-rift clastic depositional systems towards the tip of major fault segment, Suez Rift, Egypt. *Basin Research*, 14, 1–23.

Zelilidis, A. (2003) The geometry of fan-deltas and related turbidites in narrow linear basin. *Geological Journal*, *37*, 1–16.

Zelilidis, A. and Kontopoulos, N. (1996) Significance of fan deltas without toe-sets within rift and piggyback basins: examples from the Corinth graben and the Meso-hellenic though, Central Greece. *Sedimentology*, *43*, 253–262.

SUPPORTING INFORMATION

Additional supporting information may be found online in the Supporting Information section.